



Subduction-related mafic to felsic magmatism in the Malayer–Boroujerd plutonic complex, western Iran

Reza Deevsalar¹ · Ryuichi Shinjo² · Jean P. Liégeois³ · Mohammad V. Valizadeh⁴ · Jamshid Ahmadian⁵ · Hadi Yeganehfar⁵ · Mamoru Murata⁶ · Iain Neill⁷

Received: 24 April 2017 / Accepted: 23 November 2017 / Published online: 25 January 2018
© Swiss Geological Society 2018

Abstract

The Malayer–Boroujerd plutonic complex (MBPC) in western Iran, consists of a portion of a magmatic arc built by the northeast verging subduction of the Neo-Tethys plate beneath the Central Iranian Microcontinent (CIMC). Middle Jurassic-aged felsic magmatic activity in MBPC is manifested by I-type and S-type granites. The mafic rocks include gabbroic intrusions and dykes and intermediate rocks are dioritic dykes and minor intrusions, as well as mafic microgranular enclaves (MMEs). MBPC Jurassic-aged rocks exhibit arc-like geochemical signatures, as they are LILE- and LREE-enriched and HFSE- and HREE-depleted and display negative Nb–Ta anomalies. The gabbro dykes and intrusions originated from metasomatically enriched garnet-spinel lherzolite [Degree of melting (f_{mel}) \sim 15%] and exhibit negative Nd and positive to slightly negative $\varepsilon_{\text{Hf}}(\text{T})$ (+ 3.0 to – 1.6). The data reveal that evolution of Middle Jurassic magmatism occurred in two stages: (1) deep mantle-crust interplay zone and (2) the shallow level upper crustal magma chamber. The geochemical and isotopic data, as well as trace element modeling, indicate the parent magma for the MBPC S-type granites are products of upper crustal greywacke (f_{mel} : 0.2), while I-type granites formed by partial melting of amphibolitic lower crust (f_{mel} : 0.25) and mixing with upper crustal greywacke melt in a shallow level magma chamber [Degree of mixing (f_{mix}): 0.3]. Mixing between andesitic melt leaving behind a refractory dense cumulates during partial crystallization of mantle-derived magma and lower crustal partial melt most likely produced MMEs (f_{mix} : 0.2). However, enriched and moderately variable $\varepsilon_{\text{Nd}}(\text{T})$ (– 3.21 to – 4.33) and high ($^{87}\text{Sr}/^{86}\text{Sr}$)_i (0.7085–0.7092) in dioritic intrusions indicate that these magmas are likely experienced assimilation of upper crustal materials. The interpretations of magmatic activity in the MBPC is consistent with the role considered for mantle-derived magma as heat and mass supplier for initiation and evolution of magmatism in continental arc setting, elsewhere.

Keywords Zagros Orogen · Tethyan subduction zone setting · Middle Jurassic · Mantle melting · Magma mixing · Crustal anatexis

1 Introduction

Studies of the magmatic rocks formed above continental subduction zones have established that the subduction process is an, if not the, most important principal process

for the petrological-geochemical evolution of the continental crust (Anderson 2007; Grove et al. 2002; Kelemen et al. 2003; Kessel et al. 2005; O'Neill and Jenner 2012; Stracke 2012). Annen et al. (2006) further demonstrated that the chemical diversity of arc magmas is intimately tied to the processes that occur within the deep crust, while textural diversity is more commonly attributed to shallow-level crystallization processes. In this regard, the common association of mafic, intermediate and felsic rocks is likely to provide geochemical and isotopic constraints on mantle and on both deep and shallow crustal petrogenetic processes (Liankun and Kuirong 1991; Dai et al. 2011; Zhao et al. 2015). The Malayer–Boroujerd Plutonic Complex (MBPC) is an example of a plutonic suite formed above a

Editorial Handling: E. Gnos.

Electronic supplementary material The online version of this article (<https://doi.org/10.1007/s00015-017-0287-y>) contains supplementary material, which is available to authorized users.

✉ Reza Deevsalar
Deevsalar@modares.ac.ir

Extended author information available on the last page of the article

continental subduction zone, with contemporaneous occurrence of mafic, intermediate, and felsic rocks. This complex is located in the Mesozoic–Cenozoic Sanandaj–Sirjan Zone (SaSZ), one of the two magmatic zones trending parallel to one another in the Zagros Orogen (Fig. 1a, b). The SaSZ represents the internal magmatic/metamorphic part of the Zagros orogenic belt. The other magmatic zone is Cenozoic Urumieh–Dokhtar Magmatic Arc (UDMA). These zones formed by prolonged NE-

dipping subduction of Neo-Tethyan oceanic crust beneath the Central Iranian Micro-Continent (CIMC) (Fig. 1a). The Zagros Main Thrust (ZMT) marks the suture zone between the Arabian plate and the Central Iran Micro-Continent (CIMC) marking the closure of the Neo-Tethys Ocean (e.g. Stöcklin 1968; Agard et al. 2005; Paul et al. 2006, 2010). The SaSZ extends for almost 1500 km, parallel to the ZMT (Fig. 1b) joining the Taurides–Anatolides orogenic belt in Turkey in the northwest and Esfandagheh in the southeast in

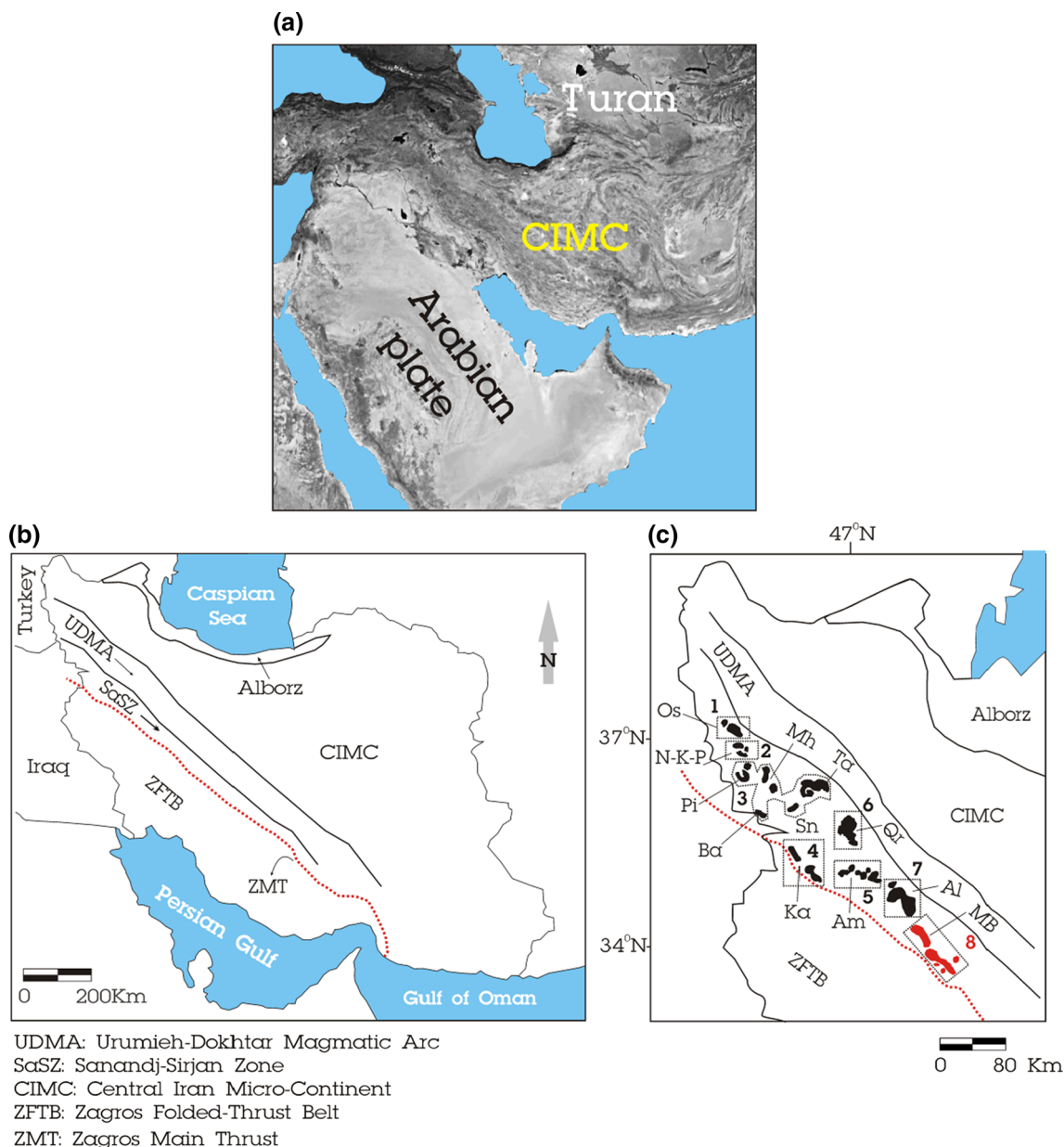


Fig. 1 **a** Landsat composite image showing the position of the CIMC between the Arabian and Turan plates (image is from Google Earth). **b** Map of Iran illustrating the location of SaSZ within the Zagros Orogeny, W Iran (adapted from Deevsalar et al. 2014). The Zagros Folded-Thrust Belt (ZFTB), Sanandaj–Sirjan Zone (SaSZ), and the Urumieh–Dokhtar Magmatic Arc (UDMA) are three major

subdivision of Zagros Orogen. **c** Simplified map of NW Iran showing the distribution of magmatic complexes in the northern SaSZ. 1-Oshnavieh and Urumieh (Os), 2-Naghade-Khalfe-Pasveh (N-K-P); 3-Piranshahr (Pi), Saqqez, Takab (Ta), Miandoab, Mahabad (Mh), Sanandaj (Sn) and Baneh (Ba); 4-Qorveh (Qr); 5-Kamyaran (Ka); 6-Almoghlagh (Al); 7-Alvand (Al); 8-Malayer–Boroujerd (MB)

Iran. During Middle Jurassic to Cretaceous time, the SaSZ represented an Andean-type margin with abundant calc-alkaline plutonic and minor preserved volcanic activities (e.g. Stöcklin 1968; Berberian and King 1981; Ghasemi and Talbot 2006; Azizi and Jahangiri 2008; Mohajjel and Fergusson 2014). In many localities within the SaSZ, intrusive rocks have been emplaced within metasedimentary units. Regional low pressure metamorphism preceded contact metamorphism associated with abundant Middle-Late Jurassic intrusions, the latter marked by widespread schists and hornfels with andalusite, sillimanite, cordierite, and garnet porphyroblasts and some exposures of marble or skarns throughout the SaSZ.

Within the northern SaSZ (N-SaSZ), the magmatic rocks are mainly plutonic and only minor volumes of volcanic rocks are reported, with the exception of the Cretaceous volcanic activities present from Sanandaj to Saqqez (Fig. 1c), in the NW-SaSZ (Azizi and Jahangiri 2008; Moinevaziri et al. 2014). This magmatism formed in two episodes during the Mesozoic: the first began in the Middle to Late Jurassic (Ahmadi-Khalaji et al. 2007; Ahadnejad et al. 2010; Vousoughi Abedini 2010; Shahbazi et al. 2010; Mahmoudi et al. 2011) and the second episode during the Middle to Late Cretaceous (Azizi and Jahangiri 2008; Azizi and Asahara 2013; Azizi et al. 2014, 2015); only one magmatic episode occurred during the Cenozoic (Late Eocene) (Mazhari et al. 2011; Mahmoudi et al. 2011; Sepahi et al. 2014; Deevsalar et al. 2017).

A large number of geochronological and geochemical studies on the SaSZ magmatic rocks testify to their derivation from Neo-Tethyan plate subduction beneath the Central Iranian Micro-Continent (CIMC) during the Mesozoic, a magmatic episode that ultimately ended with the collision between the CIMC and the Afro-Arabian plate in Cenozoic times (e.g. Ahmadi-Khalaji et al. 2007; Hassanzadeh et al. 2008; Omrani 2008; Ghalamghash et al. 2009a, b; Shahbazi et al. 2010; Ahadnejad et al. 2010; Mahmoudi et al. 2011; Esna-Ashari et al. 2012; Azizi and Asahara 2013; Chiu et al. 2013). Most of the geochemical studies in the SaSZ have focused on voluminous felsic (granitic) plutons. Comparatively few studies have been conducted on the much less abundant intermediate-mafic (diorite-gabbro) rocks (e.g. Ahmadi-Khalaji et al. 2007; Ghaffari et al. 2013; Ghalamghash et al. 2003; Mazhari et al. 2011; Sepahi 2008; Kheirkhah et al. 2013; Deevsalar et al. 2014, 2017). Yet, mafic intrusions (gabbroic dykes, mafic mega-enclaves, mafic microgranular enclaves and mafic patches) provide opportunities to explore the original traits of the mantle source region by being compositionally closer to the source than differentiated felsic rocks.

The objective of this study is to consider the whole spectrum of compositions in the MBPC from the northern

Sanandaj–Sirjan Zone (N-SaSZ). In some localities, the MBPC felsic magma chambers have been intruded by mafic magmas now preserved as dykes, microgranular enclaves and isolated patches and small stocks. These different facies have been sampled and studied, in addition to the main felsic phases. In addition to field relationships and petrographical observations, the studied rocks have been newly analyzed for major and trace elements and Sr–Nd–Hf isotopes, with data added from both published and unpublished papers. This body of data allows us to place fundamental constraints on the relationship between felsic and mafic magmatism and potential geodynamic triggers of magmatic activities in the MBPC.

2 Rock types and field relations in the MBPC

The MBPC contains both magmatic rocks and metamorphic country rocks (Fig. 2). Magma emplacement generated contact metamorphic aureoles containing andalusite or garnet, with hornfelsic textures closest to the igneous bodies. The metamorphic units, known as the Jurassic Hamadan Series, include low- to high-grade metasedimentary rocks overprinted by contact metamorphism, consisting of slate, phyllite, and spotted schist (Berthier 1974, Masoudi 1997). The intrusive rocks are plutons, stocks, and irregular-shaped ‘patches’ that together with metamorphic country rocks form a band of NW–SE trending outcrops over an elongated area that is 10 km wide and 100 km long (Fig. 2). The MBPC felsic magmatic facies comprise granodiorite, monzogranite, syenogranite, quartz diorite, monzonite, quartz monzonite, as well as aplitic, pegmatitic and silicic dykes or veins, and felsic microgranular enclaves (Ahmadi-Khalaji et al. 2007; Ahadnejad et al. 2010, 2011; Yeganehfar and Deevsalar 2016). The intermediate rocks are dioritic intrusions and dykes as well as mafic microgranular enclaves (MME). The MBPC mafic suite is also composed of gabbroic intrusions and gabbroic dykes. In the case of the MBPC mafic suites, no relationship has been observed at outcrop scale between the mafic dykes and the mafic bodies. The gabbroic intrusions have not been observed in direct contact with granitoids and they are not cross-cut by gabbro-dioritic dykes. According to published age data, the MBPC granitoids belong to the Middle Jurassic (zircon U–Pb ages of NW-MBPC 162–187 Ma; Ahadnejad et al. 2010; SE-MBPC: 169–172 Ma; Ahmadi-Khalaji et al. 2007). These Middle Jurassic ages are consistent with zircon U–Pb ages for subduction-related mafic and felsic magmatism throughout the SaSZ (Ahmadi-Khalaji et al. 2007; Ahadnejad et al. 2010; Mahmoudi et al. 2011; Esna-Ashari et al. 2012; Chiu et al. 2013; Sepahi et al. 2014).

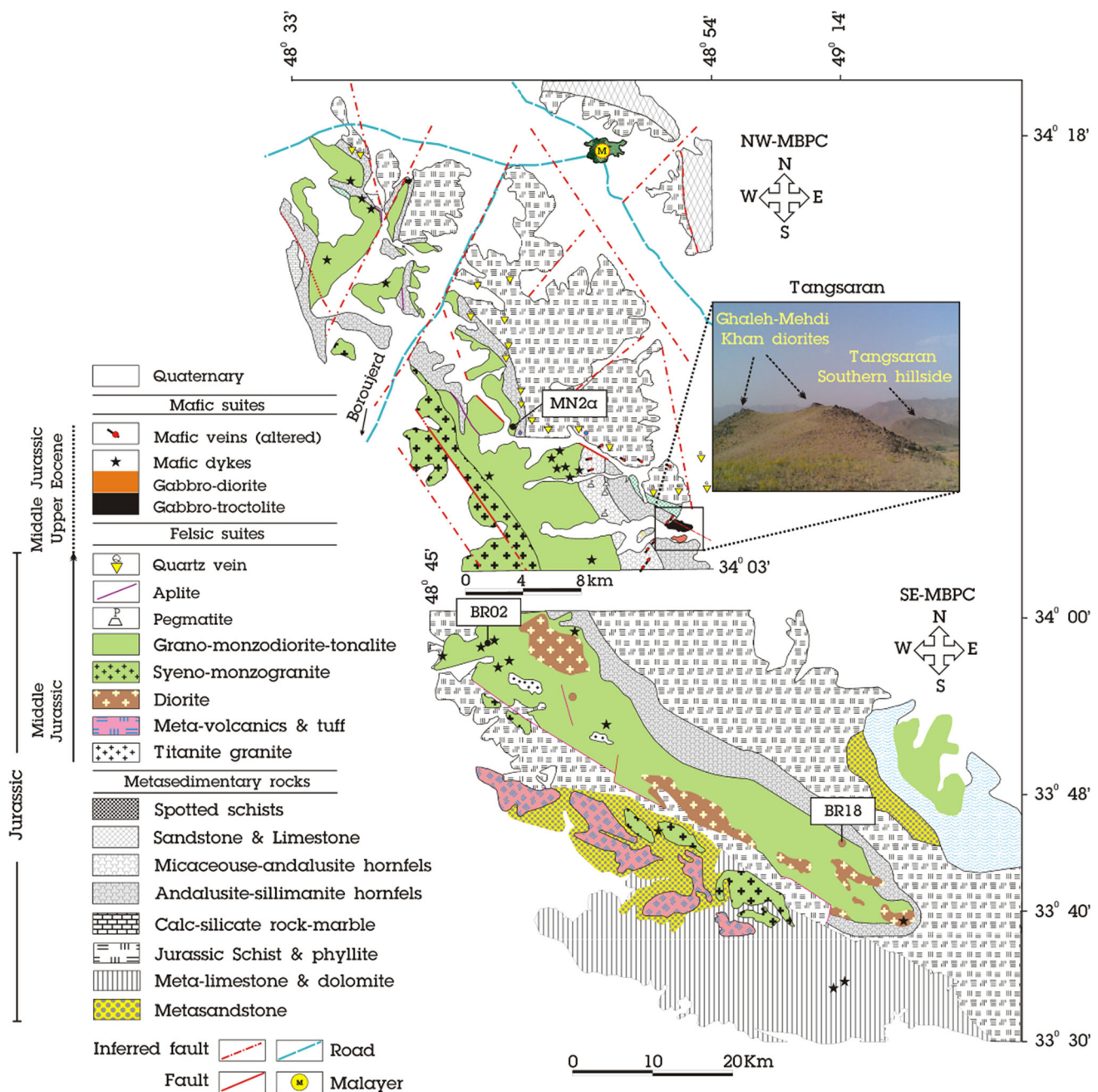


Fig. 2 Simplified geological map of the northwestern (NE-MBPC) and southeastern parts (SE-MBPC) of the Malayer–Boroujerd Plutonic complex. The inset shows the outcrop of the gabbroic rocks (Tangsaran) and gabbro-dioritic dykes (Ghaleh-Mehdi Khan)

2.1 Felsic rocks

2.1.1 Granitoids

Similar to other localities in the N-SaSZ, the MBPC granitoids are emplaced within the metamorphic rocks described above. They display generally sharp, sometimes ductile contacts with adjacent metamorphic bodies. In some locations, the presence of refractory metamorphic minerals (e.g. garnet and andalusite) inside the immediate

contact with granitic bodies reflects partial melting and assimilation of metamorphic country rocks. Granodiorite is the dominant and most widespread rock-type in both NW- and SE-MBPC area. It is frequently associated with quartz-diorite (especially in SE-MBPC) and tonalite at outcrop scale. This magmatic association displays fine- to coarse-grained granular textures comprising plagioclase (30–55%), biotite (5–30%), quartz (20–35%), and alkali feldspar (5–45%) as major phases and apatite (often as needle-like crystals in alkali feldspar), zircon, rutile,

allanite, and Fe–Ti-oxides as common accessory minerals. Biotite gives a weak to sharply foliated texture to mylonitic facies. Granodiorite usually presents microgranular centimeter- to meter-size enclaves, as well as sedimentary xenoliths (metapelitic and micaceous enclaves). Refractory minerals such as andalusite and garnet locally occur in granodiorite close to the contacts with spotted schists and hornfelses. Tonalite is rare; occurring as mesocratic fine- to medium-grained rocks containing higher proportions of modal hornblende than of biotite. More evolved granitic rocks including syenogranite and rare alkali-granite are mainly found in the NW-MBPC. These are leucocratic, medium-grained rocks, normally with less than 5% biotite and contain restitic and metapelitic enclaves (Fig. 3a).

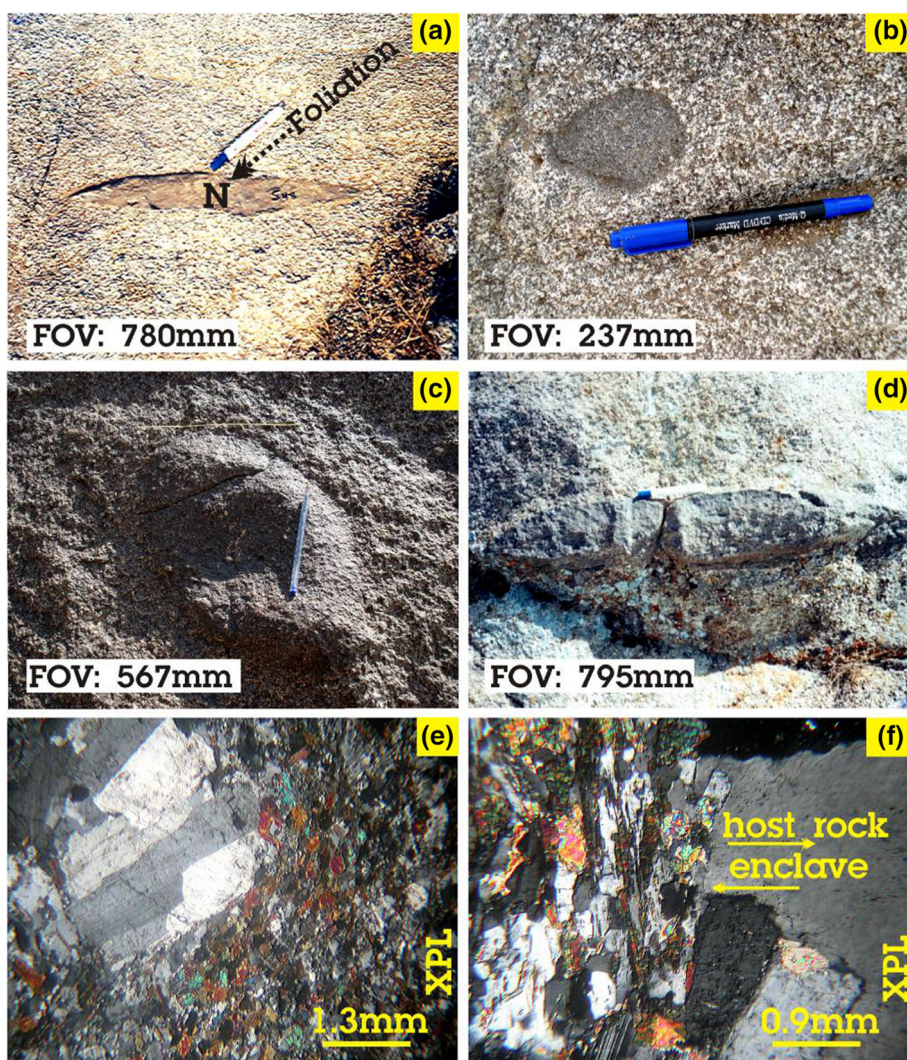
The MBPC granitoids, especially granodiorite and monzogranite, are crosscut by numerous silicic, aplitic and pegmatitic dykes and veins, marking the end of the

magmatic activity. Aplites are characterized by a fine equigranular assemblage of quartz, alkali-feldspar, some muscovite, tourmaline, and opaque oxides. Pegmatites are mainly present in granodioritic rocks and their aureoles. They show a simple mineralogy with graphic texture, with quartz, feldspar, muscovite, tourmaline, zircon, and apatite, with some andalusite and garnet in the samples crosscutting the aureoles.

2.1.2 Felsic microgranular enclaves (FME)

These enclaves are typical of plutons emplaced high in the upper crust where the temperature contrast between injected magmas and the host country rocks leads to formation of microgranitoid textures (Barbarin and Didier 1992). The MBPC felsic microgranular enclaves (FME) are dispersed in the pluton as small irregular-shaped fragments (5–50 cm

Fig. 3 **a** Weak foliation in mylonitic granite cross cut by sedimentary xenolith elongated along the magmatic flow. **b** Small rounded FME in granodioritic host. **c, d** Globular and ellipsoid-like MMEs in granodioritic host. **e, f** Linear arrangement of flaky biotite across the boundary between enclaves and host rock, indicating ductile deformation in semi-molten state



FOV: Field Of View
XPL: Crossed polarizer

in length, Fig. 3b) but generally increase toward the margins of the plutons. These cognate enclaves have similar mineral assemblages to their enclosing rocks, but display smaller grain size. The cogenetic nature of the FMEs is supported by close mineralogical and chemical composition to their host rocks (Deevsalar and Valizadeh 2010, Deevsalar et al. 2011).

2.1.3 Xenoliths

Xenoliths are pelitic in composition and are concentrated near contacts with metasedimentary units. They are closely associated with restitic or micaceous enclaves. In foliated host rocks (MBPC mylonitic rocks), they are elongated along the same direction of foliation, which is mainly given by biotite (Fig. 3a).

3 Intermediate rocks

3.1 Diorite intrusive rocks

The rare intermediate rocks in MBPC are composed of quartz diorite and diorite. They mostly occur in the SE-MBPC as separate dioritic and quartz dioritic patches and small stocks (Ahmadi-Khalaji et al. 2007) or dioritic dykes. The diorites have a subhedral granular texture and contain plagioclase and amphibole, with minor clinopyroxene and biotite. The hornblende/biotite ratio increases from quartz diorites to diorites. Titanite and apatite are accessory phases and secondary minerals are epidote, sericite, and chlorite. Quartz diorite has subhedral granular and intergranular textures and contains plagioclase, amphibole, quartz, and biotite with minor amounts of opaque minerals and orthoclase. The abundant small patches of quartz-diorite within the MBPC granodioritic plutons, especially in SE-MBPC, display sharp contacts with the enclosing host (Ahmadi-Khalaji et al. 2007).

3.2 Diorite dykes

The dioritic dykes are recognizable in the field by their grey colour, and their porphyritic texture. They are predominantly found in granodiorite and monzogranite. They are composed of 15–30 vol% plagioclase phenocrysts (2–4 mm) and amphibole (2 mm) in a 70–85% groundmass of plagioclase, amphibole, and 5% accessory minerals (including apatite, zircon, and Fe–Ti-oxides). Some samples undergone variable degrees of alteration, such as chloritization of mafic minerals and sericitization of plagioclase.

3.3 Mafic microgranular enclaves (MME)

The MMEs are most abundant in the NW-MBPC. They are found scattered throughout hornblende-biotite-bearing granitoids (granodiorite and monzogranite), but are absent in muscovite-bearing syenogranite and in the intrusions that contain large amounts of metasedimentary restite. In contrast to the irregular-shaped FMEs concentrated along the contacts of the granitic bodies (representing different pulses of magmas of felsic composition), the MMEs (Fig. 3c, d) occur in the internal parts of the granitoid plutons. At outcrop scales, MMEs are darker than the FMEs, have a finer grain-size and higher modal mafic minerals than the host granitoids. The MMEs range from a few cm to tens of cm in diameter and are roughly ellipsoid (slightly flattened) in shape. In their vicinity, plagioclase in host granitoids display linear arrangement (Fig. 3f). Mafic microgranular enclaves are classified as hornblende diorite, pyroxene diorite, and quartz diorite. They have poikilitic, equigranular, fine-grained and occasionally porphyritic textures with plagioclase phenocrysts (Fig. 3e). The MMEs contain higher proportions of ferromagnesian phases (mm-sized hornblende and pyroxene) and plagioclase and lower percentages of acidic phases (quartz and K-feldspar) than those of the host rocks. The wide range of intermediate to mafic compositions is reflected in the abundances of plagioclase (35–60 vol%), K-feldspar (0–5%), quartz (0–7%), hornblende (10–30%), biotite (0–10%) and clinopyroxene (0–5%). Biotite contains euhedral crystals of zircon and acicular apatite with rutile as inclusions. As shown in Fig. 3e, f, flaky biotite and tabular plagioclase lie parallel to boundary surface of enclave and host. The chemical differences between MMEs and host granitoids result from the relatively higher ratio of hornblende/biotite in the former.

4 Mafic rocks

Plutonic rocks of mafic composition are exposed in outcrops of various sizes between the main felsic bodies or at their margins, forming gabbroic stocks, patches (i.e. irregularly shaped intrusions), dykes (and rarely as mafic veins). Field evidence and rock type mapping indicate that intrusions of mafic composition increase in volume from the internal part of the MBPC toward its eastern margin.

4.1 Gabbro dykes

The gabbroic dykes are recognizable in the field by their grey to black colour and their fine-grained texture and mm-size phenocrysts (Fig. 4a, b). They are hornblende-bearing

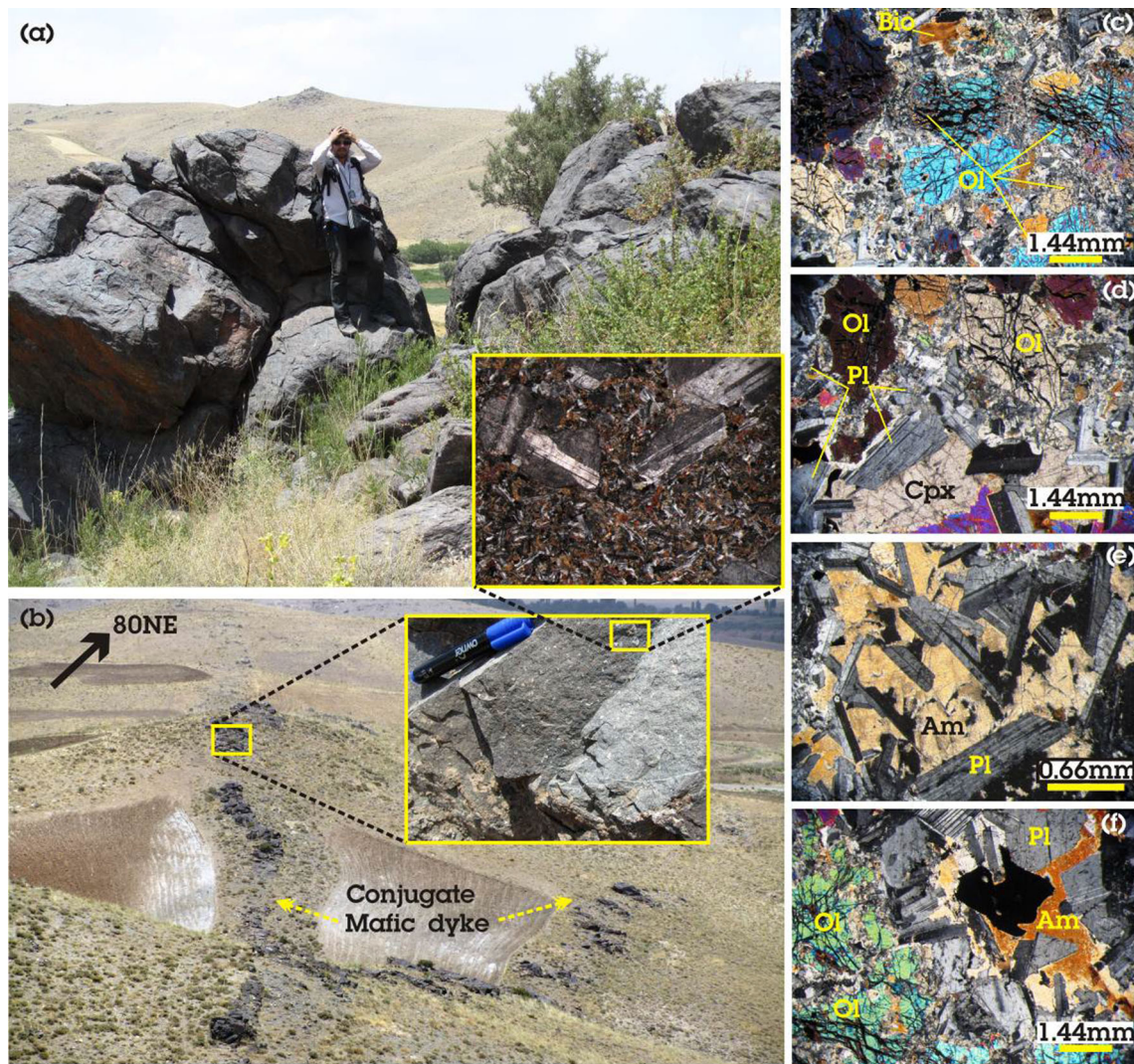


Fig. 4 a, b Two outcrops of the MBPC mafic dykes are shown. c Olivine gabbro. d Olivine-clinopyroxene gabbros. e Olivine-free hornblende gabbro with poikilitic hornblende and f hornblende-bearing olivine gabbro

pyroxene gabbro (Streckeisen and Le Maitre 1979), with a fine-grained to porphyritic texture (mm-size phenocrysts) and pale-green to gray colour. They are predominantly found in host granodioritic and monzogranitic bodies and, rarely, intruding metamorphic rock. Mafic gabbroic dykes with fine-grained to porphyritic granular texture are composed of 0–25 vol% medium- to coarse-grained plagioclase phenocrysts (2–4 mm) and medium-grained clinopyroxene and amphibole (2 mm) in a 60–80% groundmass of plagioclase, clinopyroxene, amphibole, opaques, chlorite, and sericite. In some samples, the presence of a chlorite, actinote, and epidote paragenesis indicate local greenschist facies metamorphism. In order to avoid the problem of element mobility affecting petrogenetic interpretation, the most altered samples have been excluded from the geochemical study.

4.2 Gabbro intrusions

Within the MBPC, many mafic plutonic rocks have gabbroic mineralogy and compositions, but are found to not be mappable at the scale of Fig. 2. The recognized, 2 km² large exposure occurs at Tangsaran Hill (inset map in Fig. 2). Gabbro intrusions are found as discrete bodies either hosted within or closely spatially associated with the metamorphic units. The mafic intrusions comprise olivine gabbro and hornblende gabbro. In contrast to the olivine gabbro which is marked by reactional, symplectitic intergrowths and coronas, the hornblende gabbro displays textural equilibrium. Both facies comprise samples with cumulate texture.

The massive dolerite to olivine gabbros are fine- to medium-grained (0.1–2 mm; Hibbard 1995) rocks,

composed of olivine (35–40 vol%), plagioclase (25–40 vol%), hornblende (5–20 vol%) and clinopyroxene (5–10 vol%), orthopyroxene (0–5 vol%) \pm spinel, pyrite, apatite, ilmenite (< 1 vol%) (Fig. 4c, d, f). Highly cracked olivine displays corrosion embayments. It encloses magnetite and pyrite grains of small size (\sim 0.01 mm) that have rounded shape and are located mainly along cracks, and some small rounded spinel grains. Olivine is sometimes rimmed by a very fine symplectite of amphibole and plagioclase.

The coarse-grained olivine-free gabbro contains poikilitic amphibole and plagioclase and less abundant clinopyroxene (Fig. 4e). Small subhedral clinopyroxene contains needles of magnetite and plagioclase. Magnetite (< 1%) is the most common oxide, but rare ilmenite is present. The hornblende gabbro is dark in colour, with a fine- to medium-grained (0.2–3 mm) tabular equigranular texture to slightly porphyritic, and consists of hornblende and anorthitic plagioclase as the main phases with additional minor amounts of Fe–Ti oxides, zircon, and apatite with or without clinopyroxene. Hornblende is present as anhedral crystals (up to 2 mm), which contain inclusions of plagioclase and ilmenite. Subhedral to euhedral plagioclase (1–3 mm) does not display chemical zonation.

5 Review of whole-rock major and trace element geochemistry

The whole-rock geochemical data presented in this section results from a compilation of 85 samples from three PhD thesis including first author's MSc and PhD theses developed along the last 10 years in the study area (Ahmadi-Khalaji et al. 2007; Ahadnejad et al. 2008; Deevsalar and Valizadeh 2010; Deevsalar 2015; Supplementary Item 1; Table S1). The petrographic observations and coherent behavior of mobile elements (e.g. K and Rb) throughout the range of compositions indicating only minor alteration or sub-solidus processes, enable us to conclude that element mobility was not important in this study. The MBPC magmatic rocks including felsic granitoids, intermediate dykes and enclaves and a mafic suite comprising non-cumulate gabbroic intrusions and gabbroic dykes are plotted in AFM diagram (Fig. 5a) and $\text{FeO}_{\text{tot}}/\text{MgO}$ vs SiO_2 (Fig. 5c) indicating calc-alkaline to transitional tholeiitic character. On TAS diagram (Irvine and Baragar 1971; Fig. 5b), they display a sub-alkaline character (except one altered dyke sample with high $\text{Na}_2\text{O} + \text{K}_2\text{O}$), spanning an overall range from gabbro to granite. The MBPC gabbroic and dioritic dykes and MMEs are tholeiitic, whereas gabbroic and dioritic intrusive rocks show calc-alkaline affinity (Fig. 5c).

With respect to A/CNK values [$\text{Al}_2\text{O}_3/(\text{CaO} + \text{Na}_2\text{O} + \text{K}_2\text{O})$] or alumina saturation index (ASI), the MBPC

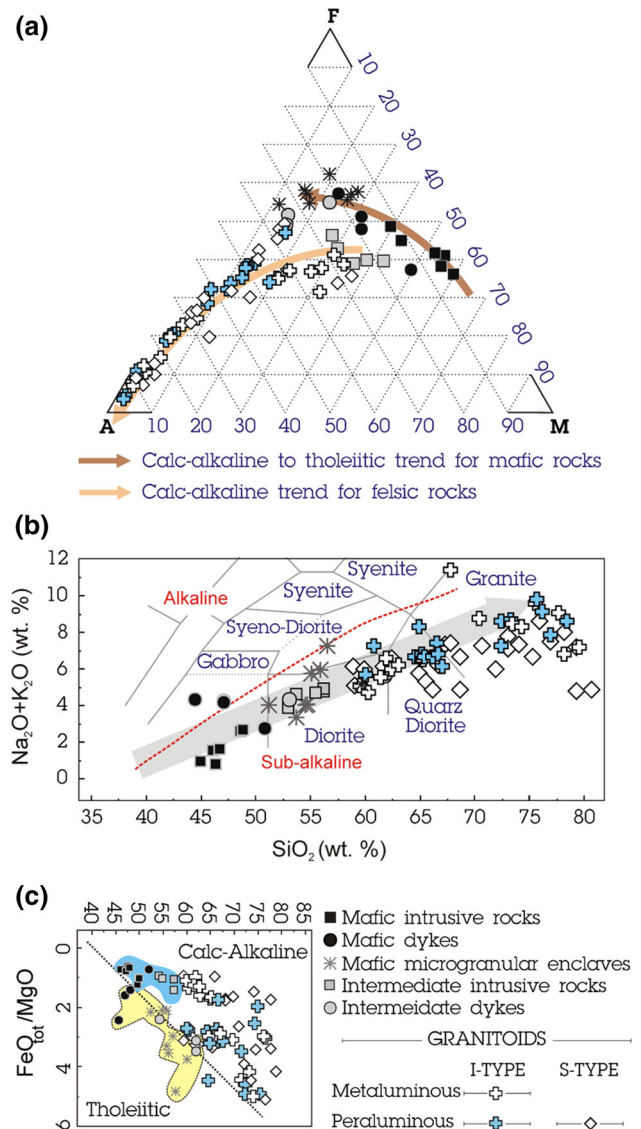


Fig. 5 Middle Jurassic rocks from the MBPC plotted on **a** AFM plot, **b** TAS diagram of Le Bas et al. (1986), **c** $\text{FeO}_{\text{tot}}/\text{MgO}$ vs SiO_2 (calc-alkaline-tholeiitic discrimination line is from Miyashiro 1974). Blue symbols are peraluminous granites (Crn-normative) and black symbols are metaluminous granites (Di-normative)

granitic rocks comprise diopside-normative, metaluminous I-type and corundum-normative, peraluminous S-type, as well as uncommon peraluminous I-type granites (Chappell and White 1974; Chappell et al. 2012). The quartz-dioritic samples and most of the granodioritic, tonalitic and monzogranitic rocks exhibit an I-type affinity ($\text{ASI} < 1.1$; Chappell 1999). Those samples containing metapelitic xenoliths have high ASI-index values and are peraluminous, S-type granites (Chappell and White 1974; Acosta-Vigil et al. 2003). In between, the syenogranites and some granodiorites and monzogranites show S-type affinity. As shown in plot of ASI-values vs. SiO_2 , the MBPC granitoids could categorize within six groups. First four groups

belongs to I-type granites (diopside-normative) and two later are S-type (corundum-normative) in composition. The areas are numbered and include: (1) evolved, and (2) less evolved I-type metaluminous granites, (3) evolved, and (4) less evolved I-type peraluminous granites, (5) evolved, and (6) less evolved S-type peraluminous granites (Fig. 6).

For a range of mafic to felsic rocks, SiO_2 (43.34–78.77 wt%) was chosen as the differentiation index because it displays the best correlations with other major oxides. Diagrams of major elements versus SiO_2 (Harker plots) appear in Fig. 7. In comparison with some important magmatic complexes of the SaSZ, including Alvand, Aligudarz, Astaneh and Siah-Kuh (Fig. 7; sources in caption), the MBPC mafic to felsic rocks cover the total range of major element variations. They conform to trends observed for similar bodies elsewhere in the SaSZ and comprise continuous trends from gabbro intrusions/dykes through MMEs and dioritic intrusions/dykes to granitic rocks. Despite the continuous trends, major oxide variations in a small range of SiO_2 concentrations for the gabbroic intrusions and dykes are not consistent with those dioritic and felsic rocks. In the plots of wt% TiO_2 and Al_2O_3 vs. wt% SiO_2 , MBPC rocks broadly show a bell-shaped pattern with decreasing TiO_2 and Al_2O_3 from 60 wt% SiO_2 , i.e. for the granitoids. This indicates a change in the cumulative minerals with greater amount of Ti-rich (such as oxides, apatite, titanite) and Al-rich (feldspar) minerals. Gabbros and gabbroic enclaves could correspond to such cumulates, but the amount of plagioclase is too low, suggesting the presence of anorthosite at depth. MnO , CaO , MgO , and FeO_{tot} concentrations significantly decrease with increasing SiO_2 (Fig. 6) in both granitoids and dioritic rocks (i.e. dykes, intrusions and MMEs). In the Na_2O and K_2O vs. SiO_2 diagram (Fig. 6), the studied rocks define roughly a bell-shaped diagram with a decreasing of K_2O at c. 68% SiO_2 , indicating the beginning of the crystallization of important amounts of

K-feldspar. Na_2O shows globally an increase with SiO_2 , but a quite large number of samples show low amounts of Na_2O (especially S-type granitoids) and a few high amounts of Na_2O (two I-type granitoids), suggesting some late-magmatic mobility of this element marked by saussurization of the plagioclase in these rocks.

Gabbroic dykes and gabbroic intrusions exhibit different compositions and trends. In the plot of SiO_2 vs TiO_2 , gabbroic dykes display high concentrations decreasing with silica, suggesting a cumulative character, while gabbroic intrusions display lower and increasing TiO_2 with increasing silica, suggesting a magmatic liquid character. MnO , CaO , Na_2O , K_2O , and FeO_{tot} contents show similar concentrations and evolutions both gabbroic types, increasing with SiO_2 . Gabbroic dykes and intrusions show quite wide variations of MgO and Al_2O_3 for a narrow range of SiO_2 . This suggests some cumulative character (olivine or Mg-enriched pyroxene and plagioclase respectively).

If compatible trace elements (Cr, Ni, and Co; Supplementary Item 3; Fig. S1a–c) can be much higher in most of the gabbroic intrusions and dykes than in the more fractionated dioritic and granitic rocks, S-types granitoids can be quite enriched, e.g. in Cr (Supplementary Item 3; Fig. S1a–c) and mafic rocks not more enriched, such as the gabbro and diorite dykes and some gabbro intrusion. This suggests that the studied rocks are already evolved, even the mafic ones; the large enrichment of the gabbros can again be attributed to a cumulative component in these rocks, probably of oxides, as already suggested by TiO_2 . Incompatible elements show different behaviors. Zirconium is increasing with SiO_2 in mafic rocks (Supplementary Item 3; Fig. S1d), except in some dykes where Zr is enriched (3–5 times at equivalent silica) and is highly variable in granitoids (70–350 ppm), with no correlation with the silica content. Rubidium and Barium show a bell-shaped pattern for most of the samples (Supplementary Item 3; Fig. S1e, f), with negative slope beginning at c. 68% SiO_2 , i.e. at the same value than K_2O . The decreasing of Rb and Ba can thus be attributed to the beginning of K-feldspar accumulation. Some samples enriched in Rb and Ba can be considered as bearing cumulative K-feldspar crystals, while the few being strongly depleted were probably affected by late magmatic processes; these samples being also very depleted in Na_2O (S-type granitoids 56, 116 and 187, 0.25 wt%, 0.19, and 0.67 wt% Na_2O , respectively). Overall, the selected samples from the MBPC have broadly arc-like features such as negative Nb–Ta anomalies, P, Ti troughs (Fig. 8a, c, e) and relatively depleted La and Nb to Ba concentration. A lack of Zr and Hf depletion (except for the dioritic intrusions) and significant Sr-depletion on normalized plots are the common features, between these rocks/groups (Fig. 8a, c, e). These rocks are also dominated by relatively enriched LREE

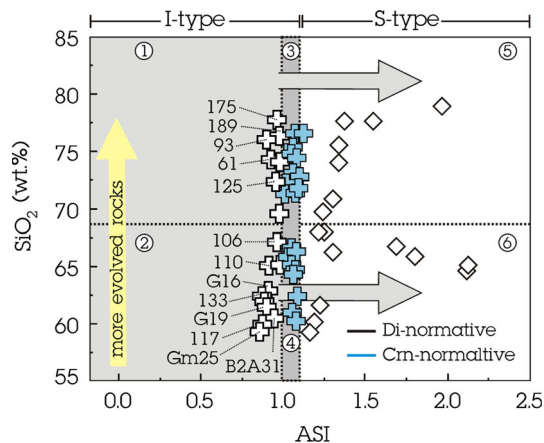
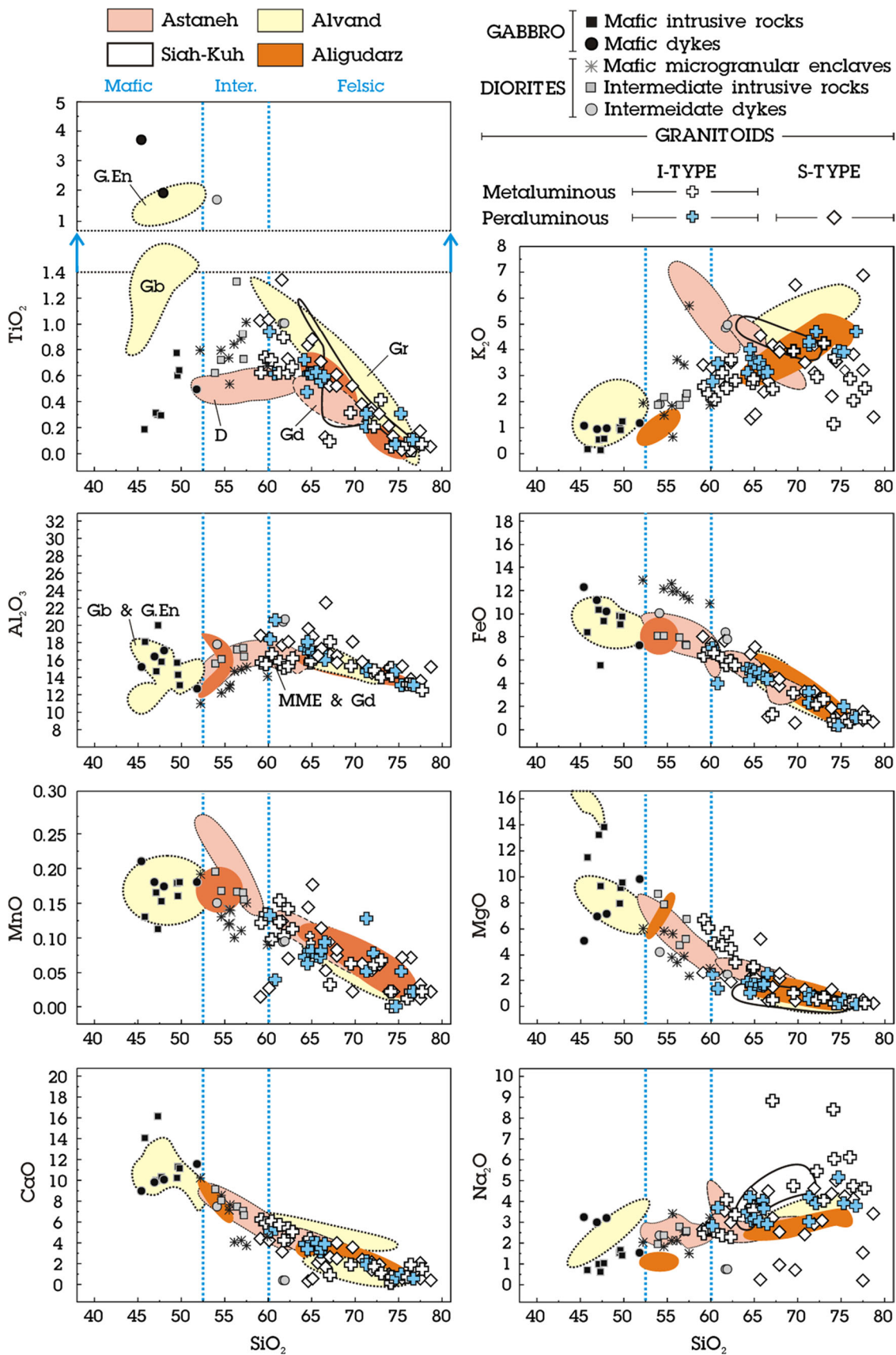


Fig. 6 Plot of SiO_2 vs. ASI-values for the MBPC granitoids



◀**Fig. 7** Major element variations with increasing SiO₂ values for MBPC gabbroic to granitic rocks. The data for granitic rocks are taken from Ahadnejad et al. (2010), Ahmadi-Khalaji et al. (2007), and data for MMEs and mafic rocks are from first author's MSc and PhD thesis and, Deevsalar et al. (2014). Alvand batholith (Ghalamghash et al. 2009b; Shahbazi et al. 2010); Aligudarz (Esna-Ashari et al. 2012); Astaneh (Tahmasbi et al. 2010); Siah-Kuh (Arvin et al. 2007). *G.En* gabbroic enclaves; *Gb* gabbro; *D* diorites; *Gd* granodiorites; *Gr* granitoids (granodiorite to syenogranites); *MME* microgranular enclaves

patters and depleted HREEs (Fig. 8b, d, f). The gabbroic intrusions have the lowest total REE-concentration ($\sum\text{REE}$ 23.8–157.8 ppm) and evolved granites possess the highest values ($\sum\text{REE}$ 70–324 ppm), even if some overlap exists. Among the MBPC magmatic rocks, the gabbroic intrusive rocks have highly variable Eu/Eu* ratios (0.49–1.77), and negative to positive Eu-anomalies, both parameters being in agreement with the variable plagioclase cumulative component noted above. Two gabbro intrusions (*M*₀₇ and *M*₁₄) have positive Eu anomaly, high Sr (up to 513 ppm) and Al₂O₃ concentrations (up to 19 wt%) indicating plagioclase accumulation. Remaining samples including gabbroic and dioritic dykes, as well as granitoids, mainly display negative (Eu/Eu* < 1) Eu-anomalies conforming to their non-cumulative character.

6 Isotopic ratios

6.1 Review Sr–Nd isotopic ratios of the MBPC granitoids

The granitic rocks from the MBPC are characterized by enriched Nd–Sr isotope compositions. They show a limited range of $\epsilon_{\text{Nd}}(\text{T}) = -2.4$ to -5.3 and initial $^{87}\text{Sr}/^{86}\text{Sr}$ [$(^{87}\text{Sr}/^{86}\text{Sr})_i = 0.7062\text{--}0.7110$ (Data from Ahadnejad et al. 2010; Ahmadi-Khalaji et al. 2007; areas 12, 13 in Fig. 9a; Supplementary Item 1; Table S2) and plot within or close to the Aligudarz granites (Esna-Ashari et al. 2012; area 9 in Fig. 9a) and the Alvand batholith (area 14 in Fig. 9a; Shahbazi et al. 2010). They have higher $\epsilon_{\text{Nd}}(\text{T})$ than those typical I- and S-type granites from south-eastern Australia (Berridale and Kosciusko batholiths, areas 9 and 11 in Fig. 9a, McCulloch and Chappell 1982) and lower than Late Jurassic Ghalaylan granitoids from N-SaSZ (Azizi et al. 2015; area 2 in Fig. 9a).

6.2 New Sr–Nd–Hf isotopic ratios for mafic rocks

New additional Nd-, Sr- and Hf-isotopic compositions of the MBPC mafic rocks are given in Tables 1 and 2. The analytical methods and procedure are in Supplementary Item 2.

6.2.1 Whole-rock Sr–Nd isotope geochemistry

The small number of new isotope ratios for gabbroic intrusions and dykes (Fig. 9a) show a limited range of compositions ($(^{87}\text{Sr}/^{86}\text{Sr})_i = 0.7052\text{--}0.7085$ and $\epsilon_{\text{Nd}}(\text{T}) = -0.1$ to -5.6 ; Fig. 9a; Table 1). These results are consistent with ratios obtained in previous studies (areas 6, 7 in Fig. 9a) indicating enriched Nd–Sr isotope compositions for both intrusions and dykes. The non-cumulate gabbro intrusions have higher $\epsilon_{\text{Nd}}(\text{T})$ than the gabbroic dykes and plot close to the Bulk Earth (similar to areas 6 in Fig. 9a). Tight data clusters in gabbroic intrusions and dykes suggest insignificant crustal contamination and retention of magmatic information despite the inevitable slight alteration or sub-solidus low grade metamorphism. The diorite intrusive rocks display lower $(^{87}\text{Sr}/^{86}\text{Sr})_i$ and higher $\epsilon_{\text{Nd}}(\text{T})$ than those of dioritic dykes (area 8 in Fig. 9a). They have similar Sr–Nd isotopic ratios which lie in the range of I-type igneous rocks. Compared to the mafic samples from across the Turkish-Iranian Plateau, the mafic magmatic rocks (areas 6 and 7 in Fig. 9a) diverge from those fields defined by younger Eocene Mafic rocks from NW Iran (Azizi et al. 2011), Upper Jurassic–Lower Cretaceous mafic rocks from the Kapan arc (Mederer et al. 2013; area 4 in Fig. 8a), and Eocene mafic rocks from N Armenia (Sahakyan et al. 2016; area 3 in Fig. 9a).

6.2.2 Whole-rock Hf-isotope geochemistry

Gabbro intrusions from the MBPC show a limited range of initial $^{176}\text{Hf}/^{177}\text{Hf}$ ratios (0.28262–0.28275) and $\epsilon_{\text{Hf}}(\text{T})$ values (-1.49 to $+2.99$), similar to the gabbro-dioritic dykes with $^{176}\text{Hf}/^{177}\text{Hf}$ ratios (0.28262–0.28273) and $\epsilon_{\text{Hf}}(\text{T})$ values (-1.56 to $+2.34$). The MBPC gabbroic intrusions and gabbro-dioritic dykes lie close to the general Hf–Nd mantle array (Fig. 9b). Comparatively few samples across the region have been analysed for Hf isotopes (Fig. 9b); all from small volume (< 5%) Cenozoic partial melts of: the convecting asthenosphere beneath Quchan, E. Iran (Kheirkhah et al. 2015) and subduction-modified lithospheric mantle beneath Mahabad in the UDMA (Neill et al. 2015), the Eslamy peninsula in the far NW of Iran (Pang et al. 2013) and Armenia (Neill et al. 2015). Compared with those samples analysed from Armenia, Quchan and Mahabad, the gabbros and gabbro-dioritic dykes are less radiogenic.

7 Discussion

The coeval occurrence of calc-alkaline mafic magmatism in proximity to intermediate and felsic types in an arc setting leads to the question of the relationship between these facies. It is possible that these samples are genetically related to one another by fractionation, assimilation or

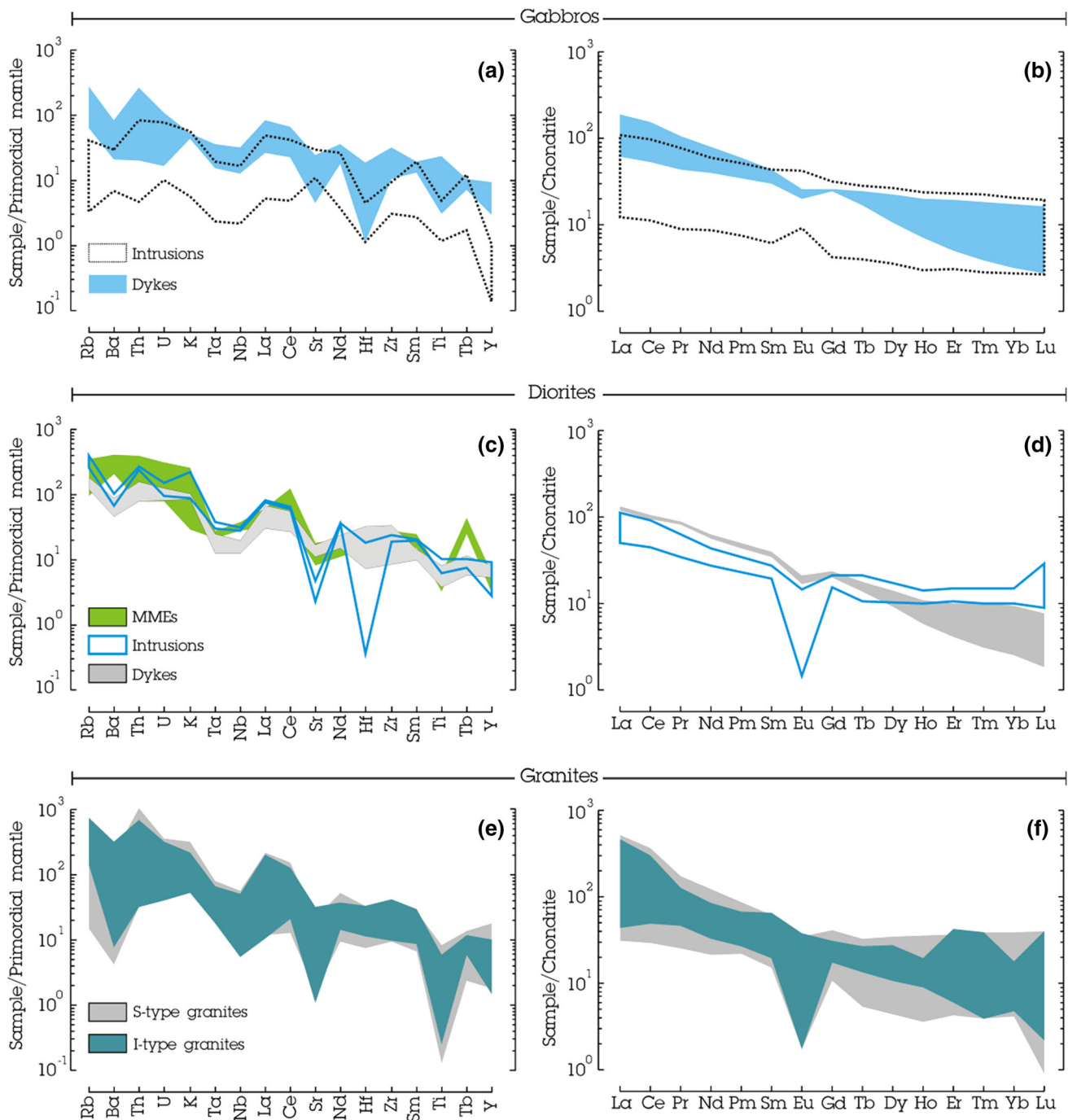


Fig. 8 Primitive mantle-normalized trace element pattern (a) and chondrite-normalized rare earth element (REE) pattern (b) of mafic rocks: gabbroic intrusions and dykes, of intermediate rocks: MMEs, dioritic intrusions and dykes (c, d), of granitic rocks (e, f). Trace

element abundances for primitive mantle are from Taylor and McLennan (1985). REE abundances for Chondrite are from Sun and McDonough (1989)

mixing processes, as perhaps implied by the geochemical continuity displayed by many of the samples and the evident interaction between mafic and felsic magmas as can be seen in many outcrops. In the following sections we focus on the spatial relationship and then potential genetic linkage between the different observed rock types.

7.1 Spatial and temporal relationship between facies

To specify the spatial relations between major rock types, we applied a graphical model using spatial analysis-kriging method in *Arc GIS 9.2*, by incorporating major element

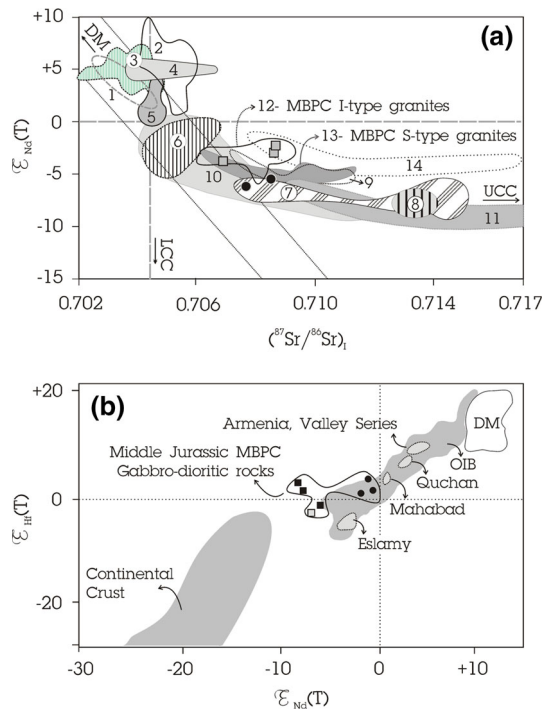


Fig. 9 Radiogenic isotope plots for MBPC mafic and felsic rocks. **a** $\epsilon_{Nd}(T)$ vs. $(^{87}Sr/^{86}Sr)_i$. The fields show, 1-Hawaii (PREMA)—Hofmann 2005; 2-Eocene Mafic rocks from NW, Iran—Azizi et al. (2011); 3-Eocene Mafic rocks from N-Armenia—Sahakyan et al. (2016); 4-Upper Jurassic–Lower Cretaceous Kapan arc—Mederer et al. (2013); 5-Ghalaylan Complex—Azizi et al. (2015); 6-MBPC Middle Jurassic gabbroic intrusive rocks, 7-MBPC Middle Jurassic gabbro dykes, and 8-MBPC Middle Jurassic dioritic dykes—(Deevsalar et al. 2014, 2017); 9-Aligudarz granites—Esna-Ashari et al. (2012); (10, 11) Berridale and Kosciusko batholiths of southeastern Australia—McCulloch and Chappell (1982); 12-MBPC I-type granites, and 13-MBPC S-type granites—Ahadnejad et al. (2010), Ahmadi-Khalaji et al. (2007); 14-Alvand granite — Shahbazi et al. (2010). **b** Eslamy samples—Pang et al. (2013); Quchan—Kheirkhah et al. (2015); Mahabad—Neill et al. (2015); Armenia, Valley Series—Neill et al. (2015). The Hf-isotopic composition of the OIB and DM are from Nowell et al. (2004), and continental crust (Vervoort et al. 1999). New data are given in Table 2

compositions determined over the past 10 years (Supplementary Item 1; Table S1). As the NW-MBPC contains a wider range of rock types and chemical composition as well as crystallization ages, it has been selected for spatial modeling. However, the gabbro-dioritic dykes have not been used in this model as they only occur within granitic bodies (Fig. 10a). The results show a sequence of geochemical/petrographical variation in NW-MBPC (Fig. 10b, c) from the eastern to the western margin. It seems that the internal part of the MBPC is composed of less evolved granitoids and those gabbro-dioritic rocks and more-evolved granites were emplaced after them at the margins. Such a model of emplacement indicates that there is a possibility the earliest emplaced granitic magmas may have been parental magma for the most highly-evolved granites.

An alternative model is that the mafic magmas are still representative of the parental magmas for the most evolved rocks, and so both these possibilities will be tested geochemically.

7.2 Petrogenesis of gabbros and gabbro-dioritic dykes

The isotopic characteristics of the MBPC gabbroic intrusions and gabbro-dioritic dykes provide valuable information concerning their origin and evolution history. Compared to felsic and intermediate rocks (i.e. granitoids and diorites; areas 12, 13 and 8 in Fig. 9a), MBPC gabbroic intrusions exhibit higher Nd- and lower Sr-isotopic ratios and they lie in the enriched part of the mantle array (area 6 in Fig. 9a). The MBPC gabbroic dykes have wider range of $(^{87}Sr/^{86}Sr)_i$ ratios which extend from mantle array to that of crustal values (areas 7, 8 in Fig. 9a). Higher Sr-isotopic ratios in some gabbroic dykes (area 7 in Fig. 9a), similar to those of dioritic dykes has been attributed to degrees of crustal contamination (Deevsalar 2015). The similar Sr- and Nd- isotopic ratios (areas 7 and 8 in Fig. 9a) as well as trace element compositions (including REE) to those dioritic dykes (Fig. 8a–d) are taken to indicate common source and similar processes involved in their petrogenesis. The low LOI-values (Ahadnejad 2009; Deevsalar 2015) and alteration indices (Supplementary Item 1; Table S1; CIA values < 50 [= molecular $[Al_2O_3/(Al_2O_3 + CaO + Na_2O + K_2O)] * 100$, suggested by Nesbitt and Young (1982)] in these gabbroic and dioritic dykes, confirm that the wide range of Sr-isotopic ratios are signaling significant crustal contamination (areas 7, 8 in Fig. 9a). Therefore, the least-contaminated and evolved samples could be used to investigate source region for middle Jurassic mafic magmatism. There is a general consensus that the majority of arc mafic magmas are generated in the mantle wedge overlying the subducting slab, through dehydration melting of metasomatised peridotite (Wilson 1989; Ulmer 2001; Grove et al. 2003). The occurrence of gabbroic samples with broadly mantle-like isotopic and geochemical compositions (high MgO, Ni, and Cr) in the MBPC (Deevsalar 2015) supports the hypothesis that melting of mantle peridotite took place. Compared to rocks derived from deep crustal sources, such as eclogite and amphibolite (Sobolev et al. 2005; Spandler et al. 2008; Wang et al. 2010), the MBPC gabbros and gabbro-dioritic dykes rocks have lower SiO_2 and higher MgO, CaO/Al_2O_3 , and Ni/MgO. The dominance of anorthitic plagioclase and Ca-rich clinopyroxene, as well as hornblende in the MBPC gabbros is also consistent with a water-rich setting like as continental subduction zone (Deevsalar et al. 2014, 2017). The enrichment in large ion lithophile element (LILE; e.g. Th, Ba, Rb), depletion in high field-strength elements

Table 1 New Sr–Nd isotopic composition of the gabbroic rocks from the MIBPC

	Rb (ppm)	Sr (ppm)	$^{87}\text{Rb}/^{86}\text{Sr}$ Measured	$^{87}\text{Sr}/^{86}\text{Sr}$ Measured	Error $\times 10^{-6}$	$^{87}\text{Sr}/^{86}\text{Sr}$ Initial	Sm (ppm)	Nd (ppm)	$^{147}\text{Sm}/^{144}\text{Nd}$ Measured	$^{143}\text{Nd}/^{144}\text{Nd}$ Measured	Error $\times 10^{-6}$	$^{143}\text{Nd}/^{144}\text{Nd}$ Initial	ϵ_{Nd} (T)
Gabbros													
Intrusions													
LM7	1.80	513.3	0.0101	0.705272	10	0.705248	1.03	4.00	0.1557	0.512557	8	0.512386	-0.70
LM8	5.10	448.3	0.0329	0.706594	8	0.706515	0.17	1.00	0.1028	0.512518	10	0.512405	-0.32
LM19	0.80	411.1	0.0056	0.705203	8	0.705190	0.45	2.00	0.1360	0.512565	10	0.512415	-0.13
Dykes													
LM40	21.10	517.4	0.1180	0.708750	9	0.708468	3.36	15.40	0.1319	0.512289	6	0.512144	-5.41
BR12	34.10	424.1	0.2327	0.708259	11	0.707703	4.52	18.70	0.1461	0.512296	8	0.512135	-5.59
Diorite													
Intrusions													
SB12	40.1	305	0.3805	0.708542	11	0.707633	5.03	38.28	0.0794	0.512290	8	0.512203	-4.28
SB10	65.02	264	0.7128	0.710123	10	0.708421	4.13	37.15	0.0672	0.512320	8	0.512246	-3.43
SM05	53.02	331	0.4636	0.709240	10	0.708133	6.25	43.60	0.0867	0.512350	8	0.512255	-3.26

These samples were analyzed at Royal Museum for Central Africa (RMCA), Tervuren (Supplementary Item 2-A)

* Standard error at the 1-sigma level

Table 2 Hf-isotope composition of the gabbro-dioritic rocks from the MBPC

	Lu (ppm)	Hf (ppm)	$^{176}\text{Lu}/^{177}\text{Hf}$ measured	$^{176}\text{Hf}/^{177}\text{Hf}$ measured	$^{176}\text{Hf}/^{177}\text{Hf}$ initial	ϵ_{Hf} today	ϵ_{Hf} (T)	Sm (ppm)	Nd (ppm)	$^{147}\text{Sm}/^{144}\text{Nd}$ measured	$^{143}\text{Nd}/^{144}\text{Nd}$ measured	ϵ_{Nd} * (T)
Intrusions												
Gabbro												
M07	0.08	0.5	0.02	0.28277	0.28270	0.11	1.34	1.03	4	0.155684	0.512557	- 0.70
BRQ2	0.14	1.08	0.02	0.28281	0.28275	1.24	3.01	1.62	7.57	0.129386	0.512515	- 0.96
BRQ1	0.38	1.01	0.05	0.28286	0.28269	3.25	0.78	5.02	27.14	0.111831	0.512418	- 2.47
M44b	0.43	1.09	0.06	0.28283	0.28264	1.95	- 0.79	-	-	-	-	-
M41b	0.50	1.06	0.07	0.28284	0.28262	2.40	- 1.54	-	-	-	-	-
BR18b	0.38	1.20	0.04	0.28281	0.28266	1.34	- 0.04	-	-	-	-	-
Dykes												
Gabbro												
MN2a	0.42	1.23	0.05	0.28279	0.28263	0.57	- 1.19	5.98	25.38	0.142455	0.512280	- 5.82
BR03b	0.41	3.30	0.02	0.28279	0.28273	0.53	2.37	6.69	37.43	0.108078	0.512140	- 7.82
MN8	0.09	0.30	0.04	0.28285	0.28271	2.83	1.58	6.25	33.6	0.112463	0.512230	- 6.16
Diorite												
BR02	0.06	0.17	0.05	0.28279	0.28262	0.71	- 1.60	7.03	38.28	0.111033	0.512160	- 7.49

These samples were analyzed at University of the Ryukyus, Japan (Supplementary Item 2-B)

* Standard error at the 1-sigma level

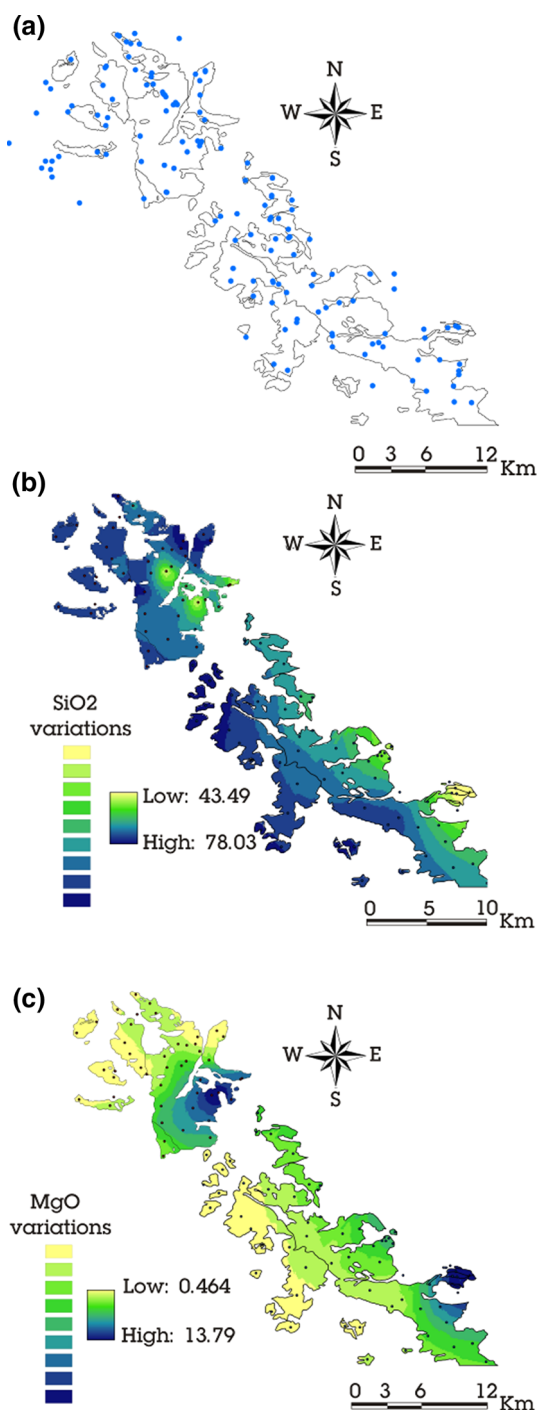


Fig. 10 Geochemical variations and spatial distribution of magmatic rocks from the NW-MBPC. **a** Sampling location and accessory points marked by small blue filled-circles. Accessory points used in blanked area to achieve a higher accuracy on neighborhood analysis. **b, c** The statistical modeling of SiO_2 and MgO -variations across the MBPC, based on spatial analysis-kriging method (Arc GIS 9.2 environment) using analyzed samples and extrapolation of neighborhood values

(HFSE; e.g. Nb, Ta, P, Zr, and Ti; Fig. 8a) coupled with low $^{87}\text{Sr}/^{86}\text{Sr}$ and positive to slightly negative ϵ_{Nd} in least-contaminated and evolved gabbros and gabbroic dykes

(Deevsalar et al. 2014; Deevsalar 2015) implies they were likely originated from sub-arc mantle wedge peridotite. In this regards, higher $^{87}\text{Sr}/^{86}\text{Sr}$ in some gabbroic dykes are attributed to significant assimilation of crustal components. Furthermore, the low Nb concentration reflected in low Nb/Y (< 3) and high K/Nb support that the mantle source were metasomatised by subduction-related fluids (Ionov et al. 2002; Verma 2006; Su et al. 2014). Given the high compatible element contents, low Rb/Sr, high Ba/Rb, and high chondrite-normalized $(\text{La}/\text{Yb})_{\text{cn}}$ and $(\text{Tb}/\text{Yb})_{\text{cn}}$ (relative HREE depletion; Fig. 8b), they were likely derived from an amphibole- and garnet-bearing mantle lherzolite. However, the $(\text{Gd}/\text{Yb})_{\text{cn}}$ ratios ranging from 1.62 to 3 indicate moderate fractionation between MREE and HREE and depth of derivation equivalent to garnet-spinel transition zone (Deevsalar 2015). The trace element modeling of melting carried out for the least-contaminated and evolved gabbros and gabbroic dykes is consistent with this hypothesis (Table 3; Fig. 11a; with parameters used in mantle melting model in Supplementary Item 1; Table S3). To investigate the source for dioritic dyke we applied mass balance calculations (Stormer and Nicolls 1978) which demonstrate that the dioritic dyke (i.e. BN_{07}) can be considered as products of fractional crystallization of mantle-derived magma (i.e. sample MN_{2a}), where the fractionated phases are Cpx (70.66 vol%), Pl (26.74 vol%), Ap (0.44 vol%), (Supplementary Item 1; Table S3). Mineral abbreviations are from Whitney and Evans (2010).

7.3 Constraints on petrogenesis of granitoids

7.3.1 S-type granites

The MBPC granitoids have isotopic, chemical, and petrological features that form two groups that should be considered separately as typical examples of I- and S-type lithologies (Chappell and White 1974). The S-type granites from the MBPC (Supplementary Item 1; Tables S1a, c, d, e; Fig. 6a) contain metapelitic xenoliths, refractory metamorphic minerals, and micaceous enclaves are considered to be products of crustal anatexis. The experiments show that the partial melting of pelite and greywacke compositions could produce up to ~ 40 vol% peraluminous granite melt at appropriate temperature (650–900 °C) (Thompson 1982; Patiño Douce and Johnston 1991a, b; Vielzeuf and Montel 1994; Montel and Vielzeuf 1997; Patiño Douce and Harris 1998), suggesting upper crustal materials as a potential source for S-type magmatism (Vielzeuf and Holloway 1988; Förster et al. 1999). Therefore, dehydration melting of upper crustal meta-greywacke/pelite (e.g. Annen et al. 2006) seems to be best simple explanation for the peraluminous S-type granites from the MBPC (area 5 in Fig. 6) which is supported by

Table 3 The results of melting and mixing model calculations

Gabbros and gabbro-dioritic dykes						Diorites →				
1	2	3	4	5	6	7	8	9	10	
	Mantle wedge Mixing		Melting	FC	FC	Melting			Mixing	
PM ^a	A ^b : 0.55F/ 0.45M	EM ^c : 80% PM + 20% A	NMBM ^d	Residual melt ^f f _{cry} = 0.45	Residual solid ^g f _{cry} = 0.35	LCC Protolith amphibolite	MFM* D _M ^h	f _{mel} = 0.25	Hybrid zone f _{mix} = 0.2 ⁱ	
Rb	0.63	71.04	4.16	27.28	54.95	8.83	24.0**	0.2	37.80	42.94
Ba	6.99	1019.20	57.60	379.26	722.95	211.27	388.0**	0.3	660.46	679.20
Th	0.09	5.10	0.34	2.22	4.91	0.81	5.0**	0.12	5.28	5.17
U	0.02	1.11	0.08	0.50	1.10	0.03	1.5**	0.02	0.00	0.33
Nb	0.71	4.64	0.91	6.01	13.08	0.39	2.3**	1.13	2.11	5.40
K	249.98	21,038.38	1289.40	8164.83	12,407.93	6288.82	11,050**	0.14	13,021.6	12,837.50
La	0.69	16.72	1.49	9.44	18.11	5.76	5.1**	1.17	4.55	8.62
Ce	1.77	34.55	3.41	20.76	39.35	12.01	22.30***	1.27	18.72	24.91
Pr	0.28	1.64	0.34	2.01	3.84	1.31	3.40***	2.51	1.61	2.28
Sr	21.10	473.80	43.73	264.40	514.15	137.15	495**	1.5	364.19	409.18
P	94.98	486.66	114.56	654.94	1438.91	10.36	3317.10***	–	–	–
Nd	1.35	15.51	2.06	11.41	20.49	6.33	11.0**	2.86	4.64	9.40
Zr	11.20	254.15	23.35	129.59	273.12	24.20	47.0**	0.25	79.32	137.46
Sm	0.44	2.79	0.56	2.77	4.78	1.84	5.0**	4.24	1.47	2.46
Eu	0.17	0.61	0.19	0.90	1.26	0.87	1.80***	4.13	0.54	0.76
Ti	1300.24	1922.51	1331.36	5682.87	10,353.85	2710.66	12,365***	4.92	3163.66	5320.72
Dy	0.74	1.60	0.78	3.11	4.88	1.78	7.80***	6.33	1.57	2.56
Y	4.55	8.81	4.77	15.10	29.65	7.36	28.0**	1.88	17.08	20.85
Yb	0.49	0.72	0.50	1.34	2.40	0.50	3.1**	4.94	0.79	1.27
Lu	0.07	0.10	0.08	0.18	0.32	0.06	0.70***	4.24	0.21	0.24
Shallow crust										
	11	12		13		14		15		16
	S-type granites					Diorites				I-type granites
	UCC Protolith greywacke ^j	Bulk D _M ^k for Melting		Melting MFM* f _{mel} = 0.2		Bulk D ^l for FC		AFC ^m R = 0.4 f _{cry} = 0.65		Mixing ⁿ (C9 + C13) ^o f _{mix} = 0.3
Rb	72.0	1.43		53.82		1.31		62.72		42.60
Ba	426.0	2.34		206.69		2.19		354.28		524.33
Th	9.0	0.1		12.55		0.12		16.14		7.46
U	2.0	0.05		0.51		0.49		2.21		0.15
Nb	8.4	1.42		6.32		1.47		9.21		3.37
K	16,602.8	0.87		18,481.58		0.85		30,224.30		14,659.59
La	34.0	0.16		66.33		0.45		39.87		23.08
Ce	58.0	0.16		111.37		0.57		78.00		46.52
Pr	6.1	0.12		9.98		0.72		8.46		4.12
Sr	201.0	0.96		207.44		2.73		158.07		317.17
P	567.3	–		–		–		–		–
Nd	25.0	0.14		44.78		0.80		33.91		16.68
Zr	302.0	0.06		177.64		0.12		673.97		108.82

Table 3 continued

	Shallow crust					
	11 S-type granites	12	13	14 Diorites	15	16 I-type granites
	UCC Protolith greywacke ^j	Bulk D_M^k for Melting	Melting MFM* $f_{mel} = 0.2$	Bulk D^l for FC	AFC ^m R = 0.4 $f_{cry} = 0.65$	Mixing ⁿ (C9 + C13) ^o $f_{mix} = 0.3$
Sm	4.6	0.14	8.46	0.98	6.73	3.57
Eu	1.2	0.6	1.72	2.05	1.30	0.90
Ti	4315.2	0.02	5.68	0.85	7663.59	2216.27
Dy	3.4	0.17	6.71	1.26	5.15	3.11
Y	26.0	0.77	31.67	1.52	23.11	21.46
Yb	2.1	0.16	4.09	0.98	3.49	1.78
Lu	0.4	0.16	0.72	0.87	0.50	0.36

Mixing equation is from Langmuir et al. (1978); Abbreviations are f_{mel} : degree of melting, f_{cry} : degree of fractionation, f_{mix} : degree of mixing

^aPM: primitive mantle composition (Sun and McDonough 1989)

^bA = Subduction sediment-derived fluids/melts. The parameters used in modeling are: normalizing values from Sun and McDonough 1989, Bulk subducted sediment composition (BOS) are from Plank and Langmuir 1998, sediment fluid partition coefficients (DSF) from Johnson and Plank (1999). Sediment melt (SM) calculated by 5% modal fractional melting of bulk subducted sediment, sediment fluids (SF) composition calculated using BOS and DSF($C_{BOS/DSF}$)

^cMiddle Jurassic Enriched Mantle

^dNMBM: Non-Modal Batch Melting

^eB = 15% partial melting of metasomatised garnet-spinel Lherzolite (Supplementary Item 3, Table S1)

^fResidual melt of fractional crystallization of 0.2 Ol + 0.05 Cpx + 0.45 Pl + 0.3 Am from B₁-magma

^gResidual solid of Fractional crystallization of 0.05 Cpx + 0.75 Pl + 0.2 Am ± 0.02 Apt from B₁-magma

^h D_M : Bulk Kd-values for amphibolite (0.7 Am + 0.3 Pl)

ⁱMixing between amphibolite partial melt and partially crystallized mantle-derived magma (^f)

^jUpper crust-greywacke composition is from Wedepohl, 1995 (35%Qtz + 30%Bio + 15% Plg + 5% Alk + 15% Mus)

^k D_M : bulk partition coefficients used in modal fractional melting of greywacke source are calculated for 0.35Qtz + 0.15Pl + 0.3Bt + 0.05Afd + 0.15Mus, Kd values for basaltic melt are taken from Rollinson 1993

^lAFC: assimilation fractional crystallization of (EM + LCC-derived melt)

^mProportions of subtracted phases: 3%Qz + 25%Bt + 55% Pl + 5% Afd + 10% Am + 2% (Zr + Apt + Mt)

ⁿMixing between LCC-derived amphibolitic melt and upper crustal melt (greywacke partial melt) in ratio of 0.7/0.03 for I-type granites

^oColumn « 9 » + column « 13 »

* MFMmodal fractional melting

** Tatsumi (2000)

*** Kogiso et al. (1997)

high ($^{87}\text{Sr}/^{86}\text{Sr}$)_i in these rocks. Worth to note that, because of small data set available for the MBPC S-type granites they exhibit relatively lower ($^{87}\text{Sr}/^{86}\text{Sr}$)_i than that of crustally contaminated gabbroic dykes. The low values (< 10) for [(Na₂O + K₂O)/(FeO_{tot} + MgO + TiO₂)], is suggestive of meta-greywacke as appropriate source for S-type granites rather than felsic pelite (Patiño Douce 1999). Trace element modeling of modal fractional melting of upper crustal greywacke also supports this scenario for the MBPC S-type granites (column « 13 » in Table 3; F_{mel} : 0.2; Fig. 11b).

7.3.2 I-type granites

I-type granites are considered to have formed by fractional crystallization of basaltic magma (Tuttle and Bowen 1958; Langmuir 1989) or partial melting of meta-igneous source (Chappell and White 1974). However, both mechanisms can lead to similar major element, trace element and isotopic characteristics in derivative magmas. The generation of igneous rocks containing more than 60 wt% SiO₂—similar to those granites from the MBPC (area 2 in Fig. 6)—requires 60% or more fractional crystallization of typical arc basalt (Foden and Green 1992; Müntener et al.

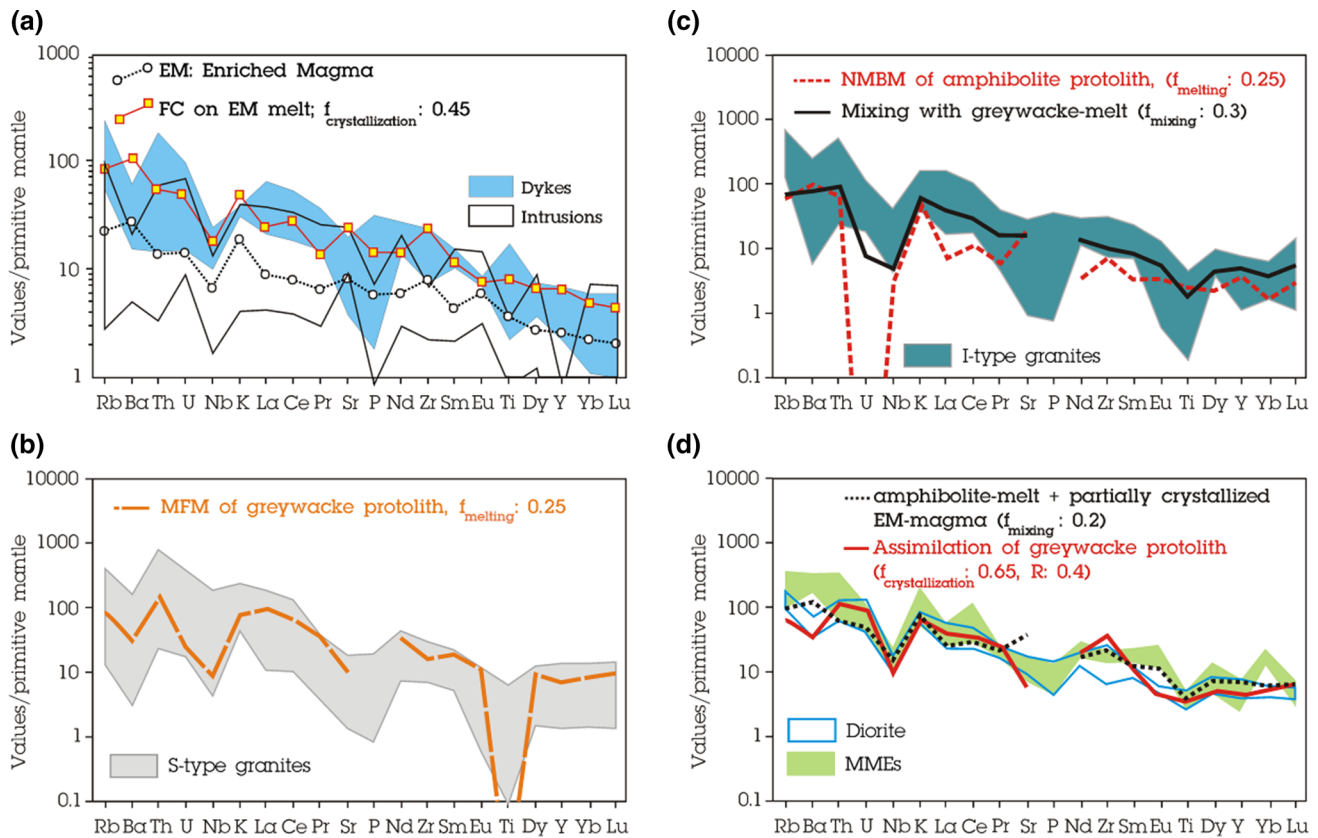


Fig. 11 **a** Non-modal batch melting curves of amphibole-bearing garnet lherzolite source and fractional crystallization (FC) on Enriched Mantle (EM). **b** Trace element modeling of melting and mixing processes for the Middle Jurassic S-type granitoids, **c** I-type granitoids, **d** MMEs and dioritic intrusions. The results of AFC model

(DePaolo 1981) are shown in Table 4. The parameters used in melting model are given in Supplementary Item 2, Table S2. *NMBM* non-modal batch melting, *MFM* modal fractional melting, F_{mixing} degree of mixing, $F_{melting}$ degree of melting and $F_{crystallization}$ degree of fractional crystallization

2001). As such, the occurrence of extensive granitic magmatism in MBPC seems to require an extraordinary volume of parental magma, which is difficult to reconcile with the low volume of mafic magmas present at shallow depth in the area. From Sr–Nd isotope geochemistry, the I-types granites are dissimilar to the mantle-derived mafic magmas. Scattering of trace element concentrations across the whole suite, however, do not reflect any genetic relationship by fractional crystallization between the various rock types (Ni and Cr vs. SiO_2 ; Supplementary Item 3; Fig. S2). The presence of MME in metaluminous I-type granites from the MBPC (Supplementary Item 1; Tables S1a–g) does indicate the contribution of mantle-derived magma as both heat and mass supplier in their magmagenesis. One popular model for the genesis of felsic rocks in arcs is by underplating of mantle-derived mafic magma, which provides sufficiently high temperatures to assist with melting of the (meta-) igneous lower crust. Based upon theoretical approaches and experimental investigations, Annen et al. (2006) demonstrate that partial crystallization of mantle-derived mafic magmas can produce residual silicic-intermediate melt and promote partial melting of refractory

lower crustal materials by transferring heat and H_2O to the deep crust. The experimental studies of Patiño Douce (1999) and Patiño Douce and McCarthy (1998) demonstrate that hydrous melting of lower crustal amphibolites or meta-basalts could produce tonalitic magmas. The derivative magmas ascend to shallow magma chamber and subsequent fractional crystallization yields granodioritic to granitic compositions. However, the presence of uncommon corundum-normative I-type granites (areas 3 and 4 in Fig. 6) and ASI-values slightly lower than unit in those metaluminous samples, as well as Sr–Nd-isotope ratios similar to those of S-type granites, invokes either homogenization by greywacke-partial melt or assimilation of meta-sedimentary crustal materials (gray horizontal arrows; Fig. 6). This scenario is supported by melting and mixing models, as shown in Fig. 11c, trace element composition of the MBPC I-type granites could be modeled as mixtures of lower crustal amphibolitic melt (column « 9 » in Table 3; f_{mel} : 0.25) and greywacke-partial melt (column « 16 » in Table 3; f_{mix} : 0.3). Lower crust-derived magmas may supply required heat for triggering upper crustal anatexis by decomposing and dehydrating of

hydrous minerals (Beard and Lofgren 1989). The final part of the emplacement model for the granitoids involves formation of a chilled contact between granitic magma and crustal wall-rock, resulting in the generation of felsic microgranular enclaves (FMEs) or felsic autoliths.

7.4 Constraints on petrogenesis of dioritic rocks

7.4.1 Diorite intrusions

Several models have been proposed for the petrogenesis of intermediate arc magmas, in which mafic magma plays an important role, namely: (1) fractional crystallization of primary basaltic magmas (Langmuir 1989), (2) extensive contamination with crustal components (Reiners et al. 1995) or assimilation and fractional crystallization of mantle-derived magma (AFC) (DePaolo 1981, Bacon and Druitt 1988), (3) mixing with crustal-derived felsic magmas (Marshall and Sparks 1984; Downes et al. 1990; Griffin et al. 2002), (4) Melting, Assimilation, Storage and Homogenisation (MASH) processes (Hildreth and Moorbath 1988), and (5) partial melting of crustal materials by thermal influence of underplated basaltic magma (e.g. Guffanti et al. 1996; Chappell and White 2001; Izbekov et al. 2004). As outlined in previous sections, the association of mafic, felsic, and intermediate rocks in the MBPC is indicative of interplay between crust and mantle. The intermediate samples display crust-like LILE and LREE enrichment (relative to HFSE and HREE), but have low silica (53.94–57.24 wt%) and high MgO (4.69–8.61 wt%) content. Petrographic observations from diorite intrusive rocks indicate the presence of sieve-textured and zoned plagioclase phenocrysts, which are generally taken as indicative of magma mixing process (Barbarin 1990; Jicha et al. 2007). In addition, the calc-alkaline dioritic intrusions from the MBPC exhibit straight-line differentiation trends in Harker plots (Fig. 7), and thus it is possible that they can be explained by mixing of mafic and felsic magmas. The composition of plagioclase changes from anorthite (for gabbros) through andesine–labradorite (for diorites) to oligoclase–andesine (for granites). The bytownite to labradorite cores in some plagioclase phenocrysts from diorites rimmed by andesine to oligoclase, indicating both mafic and silicic magmas appears to have been incorporated in their petrogenesis (Supplementary Item 1; Table S4).

As shown in Fig. 9a, $(^{87}\text{Sr}/^{86}\text{Sr})_i$ ratios of the diorite intrusions are broadly similar to the Middle Jurassic lower crust-derived I-type granites. Displacement of the dioritic intrusions away from mantle array towards crustal values indicates Sr-isotope equilibration through mixing with felsic magmas or through AFC. We argue that these diorites thus have hybrid parent magma. The multi-element

modeling shows that mixing between residual melt of high pressure fractionation of 60% Ol + 40% Cpx from enriched mantle magma (column « 6 » in Table 3; f_{cry} : 0.35) and lower crustal amphibolite-derived melt (column « 9 » in Table 3; f_{mel} : 0.25) could produce compositions similar to those of the MBPC dioritic intrusions (column « 10 » in Table 3; $f_{\text{mix}} = 0.2$). Partial crystallization of underplated mantle-derived magma and early removal of a mafic mineral assemblage drives the bulk magma towards a more silica-rich composition (e.g. Debari and Coleman 1989; Müntener et al. 2001). The hybrid andesitic melt could ascend toward high level crustal magma chamber. Trace element modeling suggest that deep-crust mixing was followed by AFC-process through assimilation of upper crustal materials (calculated using the equations of DePaolo 1981) rather than mixing with upper crustal melt (column « 15 » in Table 3; F_{cry} : 0.65; R : assimilant/melt = 0.4; Fig. 11d).

7.4.2 Mafic microgranular enclaves (MMEs)

MMEs result most often from the mingling between mafic and felsic magmas. These two magmas can have a different origin (i.e. deep crust-derived melt and mantle-derived melt; e.g. Barbarin 2005) or can belong to the same differentiation series (“endo-hybridization”; Duchesne et al. 1998). Both origins can coexist. In general, the presence of MMEs indicates the role of mafic magmas in the initiation and evolution of calc-alkaline granitoid magmas (Collins et al. 2000; Barbarin 2005). The small globular-shaped MMEs (Fig. 3c, d) in MBPC granites have an intermediate composition between gabbros and granitic rocks, similar to dioritic intrusions in terms of mineralogy and whole-rock geochemistry. They have lower silica content, higher MgO, FeO_{tot} , and compatible element concentrations (Cr, Ni, and Co) than their granitic host rocks. The MMEs contain higher hornblende/biotite, plagioclase/K-feldspar ratios and lower quartz than those of the host rocks. The contrasting modal and chemical composition to the host rocks indicates that they are not cognate magmas (Donaire et al. 2005). Chemical zoning observed in some euhedral to subhedral plagioclase crystals imply compositional disequilibrium. Compositions of the plagioclase core are similar to those of plagioclase in the gabbros (Supplementary Item 1; Tables S4b, c) and rims are broadly similar to those granodiorite and quartz diorites (Supplementary Item 1; Tables S4d), which are likely to mirror magma mixing process. On Harker diagrams, all the dioritic intrusions and MMEs together with gabbros plot along straight lines for both major and trace elements (Fig. 7; Supplementary item 3; Fig. S1). This is also interpreted as the product of mixing between mafic and felsic end-members. Sharp contacts between MMEs and their host granite, as well as a fine-

grained texture, needle-like apatite, elongated flaky biotite and aligned tabular plagioclase in MMEs, are clearly suggestive of rapid cooling and plastic deformation, implying mingling between magmas of contrasting composition, viscosity and temperature (i.e. hybrid MME and silicic host magmas). From field observations and U–Pb zircon ages, it appears that dioritic melts and some pulses of granitic magmas were emplaced simultaneously, indicating the possibility of interaction between them. These together with petrographical and geochemical evidence is conclusively in favour of mingling scenario, supporting that these dioritic MMEs are hybrid melts surrounded by felsic host magmas. This scenario is consistent with previous geochemical and microstructural studies carried out on MMEs in MBPC granites (Deevsalar and Valizadeh 2010; Deevsalar et al. 2011). Hence, similar to the dioritic intrusions, MMEs can be modeled as mixture of partially crystallized mantle magma and crustal derived melt (column « 10 » in Table 3; $f_{\text{mix}} = 0.2$), but without significant contamination by crustal materials because of their small volume and presence away from the wall rock. Given low viscosity and density, mafic melts can easily ascend to shallow level magma chambers, filled by I-type granitic magma. The contrasting viscosities between dioritic hybrid magma and granitic one only allow mingling, in which dioritic magma break up into blobs and scatter in the granitic magma to form MMEs.

8 Conclusions

The association of mantle-derived gabbros, in forms of intrusions and dykes, hybrid dioritic intrusions, MMEs and heterogeneous I-type granitic rocks from the MBPC strongly imply that the Middle Jurassic Tethyan arc in Iran was generated through the addition of mafic, mantle-derived magmas as a thermal trigger for melting of amphibolitic lower crust. Subduction-related magmatism in the MBPC occurred in two main stages: mantle–deep crust interplay, and shallow-level intracrustal processes. It begins with the synchronous mantle melting and lower crustal anatexis during the Middle Jurassic. Petrographic, geochemical, and Sr–Nd–Hf isotopic data obtained in this study together with published data, suggesting:

1. The MBPC gabbros originated from metasomatised sub-lithospheric mantle wedge peridotite with modelled amphibole-bearing lherzolite from garnet-spinel transition zone. The parental magma for the MBPC gabbros (dykes and intrusions) has been modeled at approximately 15% partial melting of this source.
2. The partial crystallization of primary mantle-derived magmas ($f_{\text{cry}}: 0.3$) occurred in the deep crust or at the

crust-mantle boundary. Significant transfer of heat and H₂O promotes melting of lower crust.

3. Metaluminous, I-type melts originated from amphibolitic lower crust ascended to shallower, upper-crustal magma reservoirs, at some point in this process supplying the requisite heat for melting of upper crustal greywacke and generation of S-type granites ($f_{\text{mel}}: 0.2$). I-type granites formed by hybridization between lower crustal amphibolite melt ($f_{\text{mel}}: 0.25$) and upper crustal greywacke melt ($f_{\text{mix}}: 0.3$).
4. MMEs are hybrid dioritic rocks formed by homogeneous mixing of partially crystallized mantle-derived magma and lower crustal silicic melt ($f_{\text{mix}}: 0.2$). They are produced by injection of hybrid magma into I-type granitic magma at high level magma chamber, magma mingling and breaking up hybrid magma into blobs which scattered in the granitic host. The assimilation of hybrid magma with upper crustal materials and subsequent fractional crystallization (AFC; $F_{\text{cry}}: 0.65$, $R: 0.4$) will produce composition similar to that of dioritic intrusions.
5. Overall, the results of this study indicate that the MBPC requires the involvement of mantle, deep and shallow crustal processes to explain fully their magmatogenesis. Middle Jurassic in N-SaSZ is the critical period in which mantle melting reached its climax, because of higher geothermal gradients associated with deep subduction of Neo-Tethys slab. However, arc-like huge felsic magmatism in N-SaSZ was likely triggered by mantle melting event, but limited outcrops of mafic plutonic rocks favor the emplacement of considerable amount of mafic magmas in depth. The presence of deep-seated large mafic intrusions requires to be investigated by geophysical evidence, in future studies.

Acknowledgements R. D. would like to acknowledge the financial support of the Ministry of Science, Research and Technology of Iran. The authors thank the reviewers for their insightful comments. We also thank Professor Lentz for his constructive suggestions, and Professor Edwin Gnos for organising the reviews and efficient handling of the manuscript.

References

- Acosta-Vigil, A., London, D., Morgan, G. B., VI, & Dewers, T. A. (2003). Solubility of excess alumina in hydrous granitic melts in equilibrium with peraluminous minerals at 700–800 °C and 200 MPa, and applications of the aluminum saturation index. *Contributions to Mineralogy and Petrology*, 146, 100–119.
- Agard, P., Omrani, J., Jolivet, L., & Mouthereau, F. (2005). Convergence history across Zagros (Iran): Constraints from collisional and earlier deformation. *International Journal of Earth Sciences*, 94, 401–419.

- Ahadnejad, V. (2009). *Petrology, geodynamic and emplacement mechanism of Malayer plutonic complex using anisotropic magnetic susceptibility (AMS)*. Ph.D. Dissertation, Tehran University, 210 pp.
- Ahadnejad, V., Valizadeh, M. V., Deevsalar, R., & Rasouli, J. (2011). The field and microstructural study of Malayer Plutonic Rocks (MPR), West Iran. *Geopersia*, 1, 59–71.
- Ahadnejad, V., Valizadeh, M. V., Deevsalar, R., & Rezaei-Kahkhaei, M. (2010). Age and geotectonic position of the Malayer granitoids: Implication for plutonism in the Sanandaj–Sirjan Zone, W Iran. *Neues Jahrbuch Fur Geologie Und Palaontologie-Abhandlungen*, 261, 61–75.
- Ahadnejad, V., Valizadeh, M. V., & Esmaeili, D. (2008). The role of Shear zone on the emplacement of Malayer Granitoid rocks, NW Iran. *Journal of Applied Sciences*, 8, 4238–4250.
- Ahmadi-Khalaji, A., Esmaeili, D., Valizadeh, M. V., & Rahimpour-Bonab, H. (2007). Petrology and geochemistry of the granitoid complex of Boroujerd, Sanandaj–Sirjan Zone, western Iran. *Journal of Asian Earth Sciences*, 29, 859–877.
- Anderson, D. L. (2007). The eclogite engine: Chemical geodynamics as a Galileo thermometer. In G. R. Foulger & D. M. Jurdy (Eds.), *Plates, Plumes and Planetary Processes*. Geological Society of America Special Paper, 430, 47–64. [https://doi.org/10.1130/2007.2430\(03\)](https://doi.org/10.1130/2007.2430(03)).
- Annen, C., Blundy, J. D., & Sparks, R. S. J. (2006). The genesis of intermediate and silicic magmas in deep crustal hot zones. *Journal of Petrology*, 47, 505–539.
- Arvin, M., Pan, Y., Dargahi, S., Malekizadeh, A., & Babaei, A. (2007). Petrochemistry of the Siah-Kuh granitoid stock southwest of Kerman, Iran: Implications for initiation of Neotethys subduction. *Journal of Asian Earth Sciences*, 30, 474–489.
- Azizi, H., & Asahara, Y. (2013). Juvenile granite in the Sanandaj–Sirjan Zone, NW Iran: Late Jurassic–Early Cretaceous arc-continent collision. *International Geology Review*, 55, 1523–1540.
- Azizi, H., & Jahangiri, A. (2008). Cretaceous subduction-related volcanism in the northern Sanandaj–Sirjan Zone, Iran. *Journal of Geodynamics*, 45, 178–190.
- Azizi, H., Najari, M., Asahara, Y., Catlos, E. J., Shimizu, M., & Yamamoto, K. (2015). U–Pb zircon ages and geochemistry of Kangareh and Taghiabad mafic bodies in northern Sanandaj–Sirjan Zone, Iran: Evidence for intra-oceanic arc and back-arc tectonic regime in Late Jurassic. *Tectonophysics*, 660, 47–64.
- Azizi, H., Tanaka, T., Asahara, Y., Chung, S.-L., & Zarrinkoub, M. H. (2011). Discrimination of the age and tectonic setting for magmatic rocks along the Zagros thrust zone, northwest Iran, using the zircon U–Pb age and Sr–Nd isotopes. *Journal of Geodynamics*, 52, 304–320.
- Azizi, H., Zanjefili-Beiranvand, M., & Asahara, Y. (2014). Zircon U–Pb ages and petrogenesis of a tonalite–trondhjemite–granodiorite (TTG) complex in the northern Sanandaj–Sirjan zone, northwest Iran: Evidence for Late Jurassic arc–continent collision. *Lithos*, 216–217, 178–195.
- Bacon, C. R., & Druitt, T. H. (1988). Compositional evolution of the zoned calc-alkaline magma chamber of Mount Mazama, Crater Lake, Oregon. *Contributions to Mineralogy and Petrology*, 98, 224–256.
- Barbarin, B. (1990). Plagioclase xenocrysts and mafic magmatic enclaves in some granitoids of the Sierra Nevada Batholith, California. *Journal of Geophysical Research*, 95, 17747–17756.
- Barbarin, B. (2005). Mafic magmatic enclaves and mafic rocks associated with some granitoids of the central Sierra Nevada batholith, California: Nature, origin, and relations with the hosts. *Lithos*, 80, 155–177.
- Barbarin, B., & Didier, J. (1992). Genesis and evolution of mafic microgranular enclaves through various types of interaction between coexisting felsic and mafic magmas. *Transactions of the Royal Society of Edinburgh: Earth Sciences*, 83, 145–153.
- Beard, J. S., & Lofgren, G. E. (1989). Effect of water on the composition of partial melts of greenstones and amphibolites. *Science*, 144, 195–197.
- Berberian, M., & King, G. C. P. (1981). Towards a paleogeography and tectonic evolution of Iran. *Canadian Journal of Earth Sciences*, 18, 210–265.
- Berthier, F. (1974). Etude stratigraphique pétrologique et structurale de la région de Khorramabad. Université de Grenoble, 281.
- Chappell, B. W. (1999). Aluminium saturation in I- and S-type granites and the characterization of fractionated haplogranites. *Lithos*, 46, 535–551.
- Chappell, B. W., Bryant, C. J., & Wyborn, D. (2012). Peraluminous I-type granites. *Lithos*, 153, 142–153.
- Chappell, B. W., & White, A. J. R. (1974). Two contrasting granite types. *Pacific Geology*, 7, 173–174.
- Chappell, B. W., & White, J. R. (2001). Two contrasting granite types: 25 years later. *Australian Journal of Earth Sciences*, 48, 489–499.
- Chiu, H. Y., Chung, S. L., Zarrinkoub, M. H., Mohammadi, S., Khatib, M. M., & Iizuka, Y. (2013). Zircon U–Pb age constraints from Iran on the magmatic evolution related to Neotethyan subduction and Zagros orogeny. *Lithos*, 162–163, 70–87.
- Collins, W. J., Richards, S. R., Healy, B. E., & Ellison, P. I. (2000). Origin of heterogeneous mafic enclaves by two-stage hybridisation in magma conduits (dykes) below and in granitic magma chambers. *Transactions of the Royal Society of Edinburgh: Earth*, 91, 27–45.
- Dai, L.-Q., Zhao, Z.-F., Zheng, Y.-F., Li, Q. L., Yang, Y. H., & Dai, M. N. (2011). Zircon Hf–O isotope evidence for crust–mantle interaction during continental deep subduction. *Earth and Planetary Science Letters*, 308, 229–244.
- Debari, S. M., & Coleman, R. G. (1989). Examination of the deep levels of an island arc: Evidence from the Tonsina ultramafic–mafic assemblage, Tonsina, Alaska. *Journal of Geophysical Research*, 94, 4373–4391.
- Deevsalar, R. (2015). *Petrology, geochemistry and tectonomagmatic evolution of mafic-intermediate rocks from the Malayer–Boroujerd plutonic complex, northern Sanandaj–Sirjan magmatic zone, Iran*. PhD Thesis, Tarbiat Modares University (TMU), Iran.
- Deevsalar, R., Ghorbani, M. R., Ghaderi, M., Ahmadian, J., Murata, M., Ozawa, H., et al. (2014). Geochemistry and petrogenesis of arc-related to intraplate mafic magmatism from the Malayer–Boroujerd plutonic complex, northern Sanandaj–Sirjan magmatic zone, Iran. *Neues Jahrbuch für Geologie and Paläontologie, Abhandlungen*, 274(1), 81–120.
- Deevsalar, R., Shinjo, R., Ghaderi, M., Murata, M., Hoskin, P. W. O., Oshiro, S., et al. (2017). Mesozoic–Cenozoic mafic magmatism in Sanandaj–Sirjan Zone, Zagros Orogen (Western Iran): Geochemical and isotopic inferences from Middle Jurassic and Late Eocene gabbros. *Lithos*, 284–285, 588–607.
- Deevsalar, R., & Valizadeh, M. V. (2010). Using field and microstructural evidence in the determination of origin of magmatic enclaves and metapelitic Xenoliths in Malayer plutonic complex West of Iran. *Scientific Quarterly Journal of Geosciences*, 19, 9–17. (in Persian, with English abstract).
- Deevsalar, R., Valizadeh, M. V., & Ahadnejad, V. (2011). Determining the nature of magmatic enclaves in granites from the Malayer plutonic complex based on geochemical and statistical methods. *Scientific Quarterly Journal of Geosciences*, 21, 129–140. (in Persian, with English abstract).
- DePaolo, D. J. (1981). Neodymium isotopes in the Colorado Front range and crust–mantle evolution in the Proterozoic. *Nature*, 291, 193–196.

- Donaire, T., Pascual, E., Pin, C., & Duthou, J. L. (2005). Microgranular enclaves as evidence of rapid cooling in granitoid rocks: The case of the Los Pedroches granodiorite, Iberian Massif, Spain. *Contribution Mineralogy and Petrology*, *149*, 247–265.
- Downes, H., Dupuy, C., & Leyrelop, A. F. (1990). Crustal evolution of the Hercynian belt of Western Europe: Evidence from lower-crustal granulitic xenoliths (French Massif Central). *Chemical Geology*, *83*, 209–231.
- Duchesne, J. C., Berza, I. T., Liégeois, J. P., & Vander, Auwera J. (1998). Shoshonitic liquid line of descent from diorite to granite: The late Precambrian post-collisional Tismana pluton (South Carpathians, Romania). *Lithos*, *45*, 281–303.
- Esna-Ashari, A., Tiepolo, M., Valizadeh, M. V., Hassanzadeh, J., & Sepahi, A. A. (2012). Geochemistry and zircon U-Pb geochronology of Aligoodarz granitoid complex, Sanandaj–Sirjan zone, Iran. *Journal of Asian Earth Sciences*, *43*, 11–22.
- Foden, J. D., & Green, D. H. (1992). Possible role of amphibole in the origin of andesite: Some experimental and natural evidence. *Contributions to Mineralogy and Petrology*, *109*, 479–493.
- Förster, H. J., Tischendorf, G., Trumbull, R. B., & Gottesman, B. (1999). Late-collisional granites in the Variscan Erzgebirge, Germany. *Journal of Petrology*, *40*, 1613–1645.
- Ghaffari, M., Rashidnejad-Omran, N., Dabiri, R., Chen, B., & Santos, J. F. (2013). Mafic–intermediate plutonic rocks of the Salmas area, northwestern Iran: Their source and petrogenesis significance. *International Geology Review*, *55*, 2016–2029.
- Ghalamghash, J., Mirnejad, H., & Rashid, H. (2009a). Mixing and mingling of mafic and felsic magmas along the Neo-Tethys continental margin, Sanandaj–Sirjan zone, NW Iran: A case study from the Alvand pluton. *Neues Jahrbuch für Mineralogie, Abhandlungen*, *186*, 79–93.
- Ghalamghash, J., Nedelec, A., Bellon, H., Vousoughi-Abedini, M., & Bouchez, J. L. (2009b). The Urumieh plutonic complex (NW Iran): A record of the geodynamic evolution of the Sanandaj–Sirjan zone during Cretaceous times- part I: Petrogenesis and K/Ar dating. *Journal of Asian Earth Sciences*, *35*, 401–415.
- Ghalamghash, J., Vousoughi-Abedini, M., Bellon, H., Emami, M. H., Pourmoafi, M., & Rashid, H. (2003). K/Ar age dating of Oshnavieh plutonic complex. *Iranian Quarterly Journal of Geosciences*, *11*, 16–27.
- Ghasemi, A., & Talbot, C. J. (2006). A new tectonic scenario for the Sanandaj–Sirjan Zone (Iran). *Journal of Asian Earth Sciences*, *26*, 683–693.
- Griffin, W. L., Wang, X., Jackson, S. E., Pearson, N. J., O'Reilly, S. Y., Xu, X. S., et al. (2002). Zircon chemistry and magma mixing, SE China: In situ analysis of Hf isotopes, Tonglu and Pingtan igneous complexes. *Lithos*, *61*, 237–269.
- Grove, T. L., Elkins-Tanton, L. T., Parman, S. W., Chatterjee, N., Muntener, O., & Gaetani, G. A. (2003). Fractional crystallization and mantle-melting controls on calc-alkaline differentiation trends. *Contributions to Mineralogy and Petrology*, *145*, 515–533.
- Grove, T., Parman, S., Bowring, S., Price, R., & Baker, M. (2002). The role of an H₂O-rich fluid component in the generation of primitive basaltic andesites and andesites from the Mt. Shasta region, N California. *Contribution to Mineralogy and Petrology*, *142*, 375–396.
- Guffanti, M., Clyne, M. A., & Muffler, L. J. P. (1996). Thermal and mass implications of magmatic evolution in the Lassen volcanic region, California, and constraints on basalt influx to the lower crust. *Journal of Geophysical Research*, *101*, 3001–3013.
- Hassanzadeh, J., Stockli, D. F., Horton, B. K., Axen, G. J., Stockli, L. D., Grove, M., et al. (2008). U–Pb zircon geochronology of late Neoproterozoic–Early Cambrian granitoids in Iran: Implications for paleogeography, magmatism, and exhumation history of Iranian basement. *Tectonophysics*, *451*, 71–96.
- Hibbard, M. J. (1995). *Petrography to petrogenesis*. New Jersey: Prentice Hall.
- Hildreth, E. W., & Moorbath, S. (1988). Crustal contributions to arc magmatism in the Andes of Central Chile. *Contributions to Mineralogy and Petrology*, *76*, 177–195.
- Hofmann, A. W. (2005). Sampling mantle heterogeneity through oceanic basalts: Isotopes and trace Elements. In R. W. Carlson (Ed.), *The mantle and core* (pp. 61–101). Amsterdam: Elsevier.
- Ionov, D. A., Bodinier, J.-L., Mukasa, S. B., & Zanetti, A. (2002). Mechanisms and sources of mantle metasomatism: Major and trace element compositions of peridotite xenoliths from Spitsbergen in the context of numerical modelling. *Journal of Petrology*, *43*, 2219–2259.
- Irvine, T. N., & Baragar, W. R. A. (1971). A guide to the chemical classification of the common volcanic rocks. *Canadian Journal of Earth Science*, *8*, 523–548.
- Izbekov, P., Gardner, J. E., & Eichelberger, J. C. (2004). Comagmatic granophyre and dacite from Karymsky volcanic center, Kamchakta; experimental constraints and magma storage conditions. *Journal of Volcanology and Geothermal Research*, *131*, 1–18.
- Jicha, B. R., Singer, B. S., Beard, B. L., Johnson, C. M., Moreno-Roa, H., & Naranjo, J. A. (2007). Rapid magma ascent and generation of 230Th excesses in the lower crust at Puyehue-Cordón Caulle, Southern Volcanic Zone, Chile. *Earth and Planetary Science Letters*, *255*, 229–242.
- Johnson, M. C., & Plank, T. (1999). Dehydration and melting experiments constrain the fate of subducted sediments. *Geochemistry Geophysics Geosystem*, *1*, 1–26.
- Kelemen, P., Hanghøj, K., & Greene, A. (2003). One view of the geochemistry of subduction-related magmatic arcs, with an emphasis on primitive andesite and lower crust. *Treatise Geochemistry*, *3*, 593–659.
- Kessel, R., Ulmer, P., Pettke, T., Schmidt, M., & Thompson, A. (2005). The water-basalt system at 4 to 6 GPa: Phase relations and second critical endpoint in a K-free eclogite at 700 to 1400 °C. *Earth and Planetary Science Letters*, *237*, 873–892.
- Kheirkhah, M., Neill, I., & Allen, M. B. (2015). Petrogenesis of OIB-like basaltic volcanic rocks in a continental collision zone: Late Cenozoic magmatism of Eastern Iran. *Journal of Asian Earth Sciences*, *406*, 19–33.
- Kheirkhah, M., Neill, I., Allen, M. B., & Ajdari, K. (2013). Small-volume melts of lithospheric mantle during continental collision: Late Cenozoic lavas of Mahabad, NW Iran. *Journal of Asian Earth Sciences*, *74*, 37–49.
- Kogiso, T., Tatsumi, Y., & Nakano, S. (1997). Trace element transport during dehydration processes in the subducted oceanic crust: 1. Experiments and implications for the origin of ocean island basalts. *Earth and Planetary Science Letters*, *148*, 193–205.
- Langmuir, C. H. (1989). Geochemical consequences of in situ crystallization. *Nature*, *340*, 199–205.
- Langmuir, C. H., Vocke, R. D., Jr., Gilbert, N. H., & Stanley, R. H. (1978). A general mixing equation with applications to Icelandic basalts. *Earth and Planetary Science Letters*, *37*, 380–392.
- Le Bas, M. J., Le Maitre, R. W., Streckeisen, A., Zanetti, B., & IUGS Subcommittee on the systematics of igneous rocks. (1986). A chemical classification of volcanic rocks based on the total alkali-silica diagram. *Journal of Petrology*, *27*, 745–750.
- Liankun, S., & Kuirong, Y. (1991). A two-stage crust-mantle interaction model for mafic microgranular enclaves in the Doning granodiorite Pluton, Guangxi, China. In J. Didier & B. Barbarin (Eds.), *Enclaves and granite petrology* (pp. 95–112). Amsterdam: Elsevier.

- Mahmoudi, S., Corfu, F., Masoudi, F., Mehrabi, B., & Mohajjel, M. (2011). U–Pb dating and emplacement history of granitoid plutons in the northern Sanandaj–Sirjan Zone, Iran. *Journal of Asian Earth Sciences*, *41*, 238–249.
- Marshall, L. A., & Sparks, R. S. J. (1984). Origin of some mixed magma and net-veined ring intrusions. *Journal of the Geological Society*, *141*, 171–182.
- Masoudi, F. (1997). *Contact metamorphism and pegmatite development in the region SW of Arak, Iran*. PhD thesis, The University of Leeds, UK.
- Mazhari, S. A., Amini, S., Ghalamghash, J., & Bea, F. (2011). Petrogenesis of granitic unit of Naqadeh complex, Sanandaj–Sirjan Zone, NW Iran. *Arabian Journal of Geosciences*, *4*, 59–67.
- McCulloch, M. T., & Chappell, B. W. (1982). Nd isotopic characteristics of S- and I-type granites. *Earth and Planetary Science Letters*, *58*, 51–64.
- Mederer, J., Moritz, R., Ulianov, A., & Chiaradia, M. (2013). Middle Jurassic to Cenozoic evolution of arc magmatism during Neotethys subduction and arc-continent collision in the Kapan Zone, southern Armenia. *Lithos*, *177*, 61–78.
- Miyashiro, A. (1974). Volcanic rock series in island arcs and active continental margins. *American Journal of Science*, *274*, 321–355.
- Mohajjel, M., & Fergusson, C. L. (2014). Jurassic to Cenozoic tectonics of the Zagros Orogen in northwestern Iran. *International Geology Review*, *56*, 263–287.
- Moinevaziri, H., Akbarpour, A., & Azizi, H. (2014). Mesozoic magmatism in the northwestern Sanandaj–Sirjan zone as an evidence for active continental margin. *Arab Journal of Geosciences*. <https://doi.org/10.1007/s12517-014-1309-y>.
- Montel, J. M., & Vielzeuf, D. (1997). Partial melting of meta-greywacke, Part II. Compositions of minerals and melts. *Contributions to Mineralogy and Petrology*, *128*, 176–196.
- Müntener, O., Kelemen, P. B., & Grove, T. L. (2001). The role of H₂O during crystallisation of primitive arc magmas under uppermost mantle conditions and genesis of igneous pyroxenites: An experimental study. *Contributions to Mineralogy and Petrology*, *141*, 643–658.
- Neill, I., Meliksetian, K., Allen, M. B., Navasardyan, G., & Kuiper, L. (2015). Petrogenesis of mafic collision zone magmatism: The Armenian sector of the Turkish–Iranian Plateau. *Chemical Geology*, *403*, 24–41.
- Nesbitt, H. W., & Young, G. M. (1982). Early Proterozoic climates and plate motions inferred from major element chemistry of lutite. *Nature*, *299*, 715–717.
- Nowell, G. M., Pearson, D. G., Bell, D. R., Carlson, R. W., Smith, C. B., Kempton, P. D., et al. (2004). Hf isotope systematics of Kimberlites and their megacrysts: New constraints on their source regions. *Journal of Petrology*, *45*, 1583–1612.
- O'Neill, H. S. C., & Jenner, F. E. (2012). The global pattern of trace-element distributions in ocean floor basalts. *Nature*, *491*, 698–704.
- Omrani, J. (2008). Arc-magmatism and subduction history beneath the Zagros Mountains, Iran: A new report of adakites and geodynamic consequences. *Lithos*, *106*, 380–398.
- Pang, K. N., Chung, S. L., Zarrinkoub, M. H., Lin, Y. C., Lee, H. Y., Lo, C. H., et al. (2013). Iranian ultrapotassic volcanism at ~ 11 Ma signifies the initiation of post-collision magmatism in the Arabia–Eurasia collision zone. *Terra Nova*, *25*, 405–413.
- Patiño Douce, A. E. (1999). What do experiments tell us about the relative contributions of crust and mantle to the origin of granitic magmas? In A. Castro, C. Fernandez & J. L. Vigneresse (Eds.), *Understanding Granites: Integrating New and Classical Techniques: Geological Society, London, Special Publications*, *168*, 55–75.
- Patiño Douce, A. E., & Harris, N. (1998). Experimental constraints on Himalayan anatexis. *Journal of Petrology*, *39*, 689–710.
- Patiño Douce, A. E., & Johnston, A. D. (1991a). Phase equilibria and melt productivity in the pelitic system: Implications for the origin of peraluminous granitoids. *Contributions to Mineralogy and Petrology*, *107*, 202–218.
- Patiño Douce, A. E., & Johnston, A. D. (1991b). Phase equilibria and melt productivity in the pelite system: Implications for the origin of peraluminous granitoids and aluminous gneisses. *Contributions to Mineralogy and Petrology*, *107*, 202–218.
- Patiño Douce, A. E., & McCarthy, T. C. (1998). Melting of crustal rocks during continental collision and subduction. In B. R. Hacker & J. G. Doc (Eds.), *When Continents Collide: Geodynamics and Geochemistry of Ultra-high Pressure Rocks* (pp. 27–55). Dordrecht: Kluwer Academic Publishers.
- Paul, A., Kaviani, A., Hatzfeld, D., Tatar, M., & Priestley, K. (2010). Seismic imaging of the lithospheric structure of the Zagros Mountain belt Iran. *Journal of Geological Society of London Special Publication*, *330*, 5–18.
- Paul, A., Kaviani, A., Hatzfeld, D., Vergne, J., & Mokhtari, M. (2006). Seismological evidence for crustal-scale thrusting in the Zagros mountain belt Iran. *Geophysical Journal International*, *166*, 227–237.
- Plank, T., & Langmuir, C. H. (1998). The chemical composition of subducting sediment and its consequences for the crust and mantle. *Chemical Geology*, *145*, 325–394.
- Reiners, P. W., Nelson, B. K., & Ghiorso, M. S. (1995). Assimilation of felsic crust by basaltic magma: Thermal limits and extents of crustal contamination of mantle-derived magmas. *Geology*, *23*, 563–566.
- Rollinson, H. R. (1993). *Using geochemical data: Evaluation, presentation, interpretation* (p. 325). Harlow: Longmans.
- Sahakyan, L., Bosch, D., Sosson, M., Avagyan, A., Galoyan, G. H., Rolland, Y., et al. (2016). Geochemistry of the Eocene magmatic rocks from the Lesser Caucasus area (Armenia): Evidence of a subduction geodynamic environment. *Geological Society, London, Special Publications*, *428*, 73–98.
- Sepahi, A. A. (2008). Typology and petrogenesis of granitic rocks in the Sanandaj–Sirjan metamorphic belt, Iran: With emphasis on the Alvand plutonic complex. *Neues Jahrbuch für Geologie und Paläontologie Abhandlungen*, *247*, 295–312.
- Sepahi, A. A., Shahbazi, H., Siebel, W., & Ranin, A. (2014). Geochronology of plutonic rocks from the Sanandaj–Sirjan Zone, Iran and new zircon and titanite U–Th–Pb ages for granitoids from the marivan pluton. *Geochronometria*, *41*, 207–215.
- Shahbazi, H., Siebel, W., Pourmoafaei, M., Ghorbani, M., Sepahi, A. A., Shang, C. K., et al. (2010). Geochemistry and U–Pb zircon geochronology of the Alvand plutonic complex in Sanandaj–Sirjan Zone Iran: New evidence for Jurassic magmatism. *Journal of Asian Earth Sciences*, *39*, 668–683.
- Sobolev, A. V., Hofmann, A. W., Sobolev, S. V., & Nikogosian, I. K. (2005). An olivine-free mantle source of Hawaiian shield basalts. *Nature*, *434*, 590–597.
- Spandler, C., Hermann, J., Faure, K., Mavrogenes, J. A., & Arculus, R. J. (2008). The importance of talc and chlorite ‘hybrid’ rocks for volatile recycling through subduction zones; evidence from the high-pressure subduction melange of new Caledonia. *Contributions to Mineralogy and Petrology*, *155*, 181–198.
- Stöcklin, J. (1968). Structural history and tectonics of Iran: A review. *Bulletin of the American Association of Petroleum Geologists*, *52*, 1229–1258.
- Stormer, J. C., & Nicolls, J. (1978). XLFAC: A program for the interactive testing of magmatic differentiation models. *Computer and Geosciences*, *4*, 143–159.

- Stracke, A. (2012). Earth's heterogeneous mantle: A product of convection-driven interaction between crust and mantle. *Chemical Geology*, 330–331, 274–299.
- Streckeisen, A. L., & Le Maitre, R. W. (1979). A chemical approximation to the modal QAPF classification of the igneous rocks. *Neues Jahrbuch für Mineralogie, Abhandlungen*, 136, 169–206.
- Su, B.-X., Chung, S.-L., Zarrinkoub, M. H., Pang, K.-N., Chen, L., Ji, W.-Q., et al. (2014). Composition and structure of the lithospheric mantle beneath NE Iran: Constraints from mantle xenoliths. *Lithos*, 202–203, 267–282.
- Sun, S. S., & McDonough, W. F. (1989). Chemical and isotopic systematics of oceanic basalts: Implications for mantle composition and processes. In A. D. Saunders & M. Norry, (Eds), *Magmatism in ocean basins. Geological Society of London Special Publication*, 42, 313–345.
- Tahmasbi, Z., Castro, A., Khalili, M., Ahmadi Khalaji, A., & de la Rosa, J. (2010). Petrologic and geochemical constraints on the origin of Astaneh pluton, Zagros orogenic belt, Iran. *Journal of Asian Earth Sciences*, 39, 81–96.
- Tatsumi, Y. (2000). Continental crust formation by crustal delamination in subduction zones and complementary accumulation of the enriched mantle I component in the mantle. *Geochemistry Geophysics Geosystems*, 1. <https://doi.org/10.1029/2000GC000094>.
- Taylor, S. R., & McLennan, S. M. (1985). *The continental crust: Its composition and evolution*. Oxford: Blackwell.
- Thompson, R. N. (1982). Magmatism of the British Tertiary volcanic province. *Scottish Journal of Geology*, 18, 49–107.
- Tuttle, O. F., & Bowen, N. L. (1958). Origin of granite in the light of experimental studies in the system NaAlSi₃O₈–KAlSi₃O₈–SiO₂–H₂O. *Mem. Geological Society America*, 74, 153.
- Ulmer, P. (2001). Partial melting in the mantle wedge—the role of H₂O in the genesis of mantle-derived ‘arc-related’ magmas. *Physics of the Earth and Planetary Interiors*, 127, 215–232.
- Verma, S. P. (2006). Extension-related origin of magmas from a garnet-bearing source in the Los Tuxtlas volcanic field, Mexico. *International Journal of Earth Science (Geol Rundsch)*, 95, 871–890.
- Vervoort, J. D., Patchett, P. J., Blichert-Toft, J., & Albarede, F. (1999). Relationships between Lu–Hf and Sm–Nd isotopic systems in the global sedimentary system. *Earth and Planetary Science Letters*, 168, 79–99.
- Vielzeuf, D., & Holloway, J. R. (1988). Experimental determination of the fluid-absent melting relations in the pelitic system. Consequences for crustal differentiation. *Contributions to Mineralogy and Petrology*, 98, 257–276.
- Vielzeuf, D., & Montel, J. M. (1994). Partial melting of metagreywackes. 1. Fluid-absent experiments and phase relationships. *Contributions to Mineralogy and Petrology*, 117, 375–393.
- Vousoughi Abedini, M. (2010). Geochemistry and U–Pb zircon geochronology of the Alvand plutonic complex in Sanandaj–Sirjan Zone Iran: New evidence for Jurassic magmatism. *Journal of Asian Earth Sciences*, 39, 668–683.
- Wang, Y., Zhang, F. F., Fan, W. M., Zhang, G. W., Chen, S. Y., Cawood, P. A., et al. (2010). Tectonic setting of the South China Block in the early Paleozoic: Resolving intracontinental and ocean closure models from detrital zircon U–Pb geochronology. *Tectonics*, 29, 6.
- Wedepohl, K. H. (1995). The composition of the continental crust. *Geochimica et Cosmochimica Acta*, 59(217–1), 239.
- Whitney, D. L., & Evans, B. W. (2010). Abbreviations for name of rock-forming minerals. *American Mineralogist*, 95, 185–187.
- Wilson, M. (1989). *Igneous petrogenesis*. Unwin Hyman Ed, London.
- Yeganehfar, H., & Deevsalar, R. (2016). Emplacement PT conditions of granitoids from the NW-part of the Malayer-Boroujerd plutonic complex, W Iran. *Journal of Tethys*, 4, 346–360.
- Zhao, Z. F., Dai, L. Q., & Zheng, Y. F. (2015). Two types of the crust-mantle interaction in continental subduction zones. *Science China: Earth Sciences*, 58, 1269–1283.

Affiliations

Reza Deevsalar¹ · Ryuichi Shinjo² · Jean P. Liégeois³ · Mohammad V. Valizadeh⁴ · Jamshid Ahmadian⁵ · Hadi Yeganehfar⁵ · Mamoru Murata⁶ · Iain Neill⁷

¹ Department of Geology, Tarbiat Modares University, Tehran 14115-175, Iran

² Department of Physics and Earth Sciences, University of the Ryukyus, Okinawa, Japan

³ Geodynamics and Mineral Resources, Royal Museum for Central Africa, Tervuren, Belgium

⁴ Department of Geology, University of Tehran, Tehran, Iran

⁵ Department of Geology, Payame Noor University (PNU), Tehran 19395-3697, Iran

⁶ Department of Geosciences, Naruto University of Education, Naruto, Japan

⁷ School of Geographical and Earth Sciences, University of Glasgow, Lilybank Gardens, Glasgow, Scotland G12 8QQ, UK